Published for SISSA by Springer

Received: June 18, 2021
Revised: September 6, 2021
Accepted: October 21, 2021
Published: November 9, 2021

Search for a heavy Higgs boson decaying into two lighter Higgs bosons in the $\tau\tau$bb final state at 13 TeV

The CMS collaboration

E-mail: cms-publication-committee-chair@cern.ch

Abstract: A search for a heavy Higgs boson H decaying into the observed Higgs boson h with a mass of 125 GeV and another Higgs boson h_S is presented. The h and h_S bosons are required to decay into a pair of tau leptons and a pair of b quarks, respectively. The search uses a sample of proton-proton collisions collected with the CMS detector at a center-of-mass energy of 13 TeV, corresponding to an integrated luminosity of 137 fb^{-1}. Mass ranges of 240–3000 GeV for m_H and 60–2800 GeV for m_{h_S} are explored in the search. No signal has been observed. Model independent 95% confidence level upper limits on the product of the production cross section and the branching fractions of the signal process are set with a sensitivity ranging from 125 fb (for $m_H = 240$ GeV) to 2.7 fb (for $m_H = 1000$ GeV). These limits are compared to maximally allowed products of the production cross section and the branching fractions of the signal process in the next-to-minimal supersymmetric extension of the standard model.

Keywords: Hadron-Hadron scattering (experiments), Higgs physics

ArXiv ePrint: 2106.10361

https://doi.org/10.1007/JHEP11(2021)057

Contents

JHEP11(2021)057

1 Introduction

The discovery of the Higgs boson (h) with a mass of 125 GeV at the CERN LHC [1–3] has turned the standard model (SM) of particle physics into a theory that could be valid up to the Planck scale. To date all properties of the observed particle are in agreement with the expectations of the SM within an experimental precision of 5–20% [4–7]. Despite its success in describing a wealth of phenomena, the SM falls short of addressing a number of fundamental theoretical questions and striking observations in nature. In this respect it is considered to be still incomplete.

Supersymmetry (SUSY) postulates a bosonic (fermionic) partner particle for each SM fermion (boson), with the same quantum numbers as the corresponding SM particle apart from its (half-) integer spin [8, 9]. The fact that to date no such SUSY particles have been observed implies that if SUSY were realized in nature it must be a broken symmetry. Apart from the prediction of a sizable number of new particles, SUSY requires the extension of the Brout-Englert-Higgs mechanism part [10–15] of the SM Lagrangian. In the minimal

supersymmetric extension of the SM (MSSM) [16, 17] one more SU(2) doublet of complex scalar fields is introduced with respect to the SM, leading to the prediction of two charged and three neutral Higgs bosons, one of which can be associated with h. A further extension of the MSSM by one additional complex scalar field S is theoretically well motivated, since it can solve the so called "μ-problem" of the MSSM [18]. It leads to the next-to-minimal supersymmetric SM (NMSSM), as reviewed, e.g., in refs. [19, 20]. Since S is a complex field, the number of predicted Higgs bosons increases by two, resulting in two charged and five neutral Higgs bosons, of which three are scalar and two are pseudoscalar in nature.

Many searches for additional Higgs bosons in the context of the MSSM have been performed by the LHC experiments. In the absence of signal, these have led to the exclusion of large parts of the MSSM parameter space for masses of the additional neutral Higgs bosons up to $\approx$2 TeV [21–24]. The parameter space of the NMSSM, on the other hand, is still largely unconstrained [25].

The current analysis focuses on the $\mathrm{H} \to \mathrm{h}\mathrm{h}_\mathrm{S}$ decay of a heavy Higgs boson H into h and another neutral boson h_S with a mass of $m_{\mathrm{h}_\mathrm{S}} < m_\mathrm{H} - m_\mathrm{h}$. It is based on the data recorded during the years 2016, 2017, and 2018 at a center-of-mass energy of 13 TeV with the CMS experiment, resulting in an integrated luminosity of 137 fb^{-1}. The search is inspired by the NMSSM, where h_S could have a dominant admixture of the additional singlet field S, leading to a significant suppression of its couplings to SM particles and thus of its direct production at the LHC. In this case, the production of H and subsequent decay into $\mathrm{h}\mathrm{h}_\mathrm{S}$ would become the dominant source for h_S production. Despite the overall reduced coupling strengths to SM particles, the branching fractions of h_S for its decay into SM particles are still expected to be similar to those of h. While here we use the NMSSM as a motivation, any other two Higgs doublet plus singlet model is equally relevant for the search.

A promising signature for the search is given by the decay of h into a pair of tau leptons and the decay of h_S into a pair of b quarks, $\mathrm{h}(\tau\tau)\mathrm{h}_\mathrm{S}(\mathrm{bb})$. For better readability we will not distinguish fermions by particle or antiparticle in this final state in subsequent notation throughout the text. The decay into b quarks is chosen for its large branching fraction. The decay into tau leptons is chosen for its cleaner signature compared to the decay into b quarks. This search is restricted to H production from gluon fusion. The Feynman diagram for the process of interest is shown in figure 1. The search is performed in the mass ranges of $240 \leq m_\mathrm{H} \leq 3000$ GeV and $60 \leq m_{\mathrm{h}_\mathrm{S}} \leq 2800$ GeV. It is the first search for such a process at the LHC. No attempt is made to identify and treat specially boosted topologies, for which the h and h_S decay products may not easily be spatially resolved. These can occur in parts of the explored mass ranges, e.g., for large values of m_H and small values of $m_{\mathrm{h}_\mathrm{S}}$. However, for the majority of the mass hypotheses that are considered, the contribution from boosted-topology events is subdominant.

The paper is organized as follows. A brief introduction of the CMS detector and event reconstruction are given in sections 2 and 3, respectively. The model used to describe the data is given in section 4. The event selection and categorization are described in section 5, followed by a discussion of the systematic uncertainties considered for the analysis of the data in section 6. The results of the search are presented in section 7. The paper is summarized in section 8.

JHEP11(2021)057

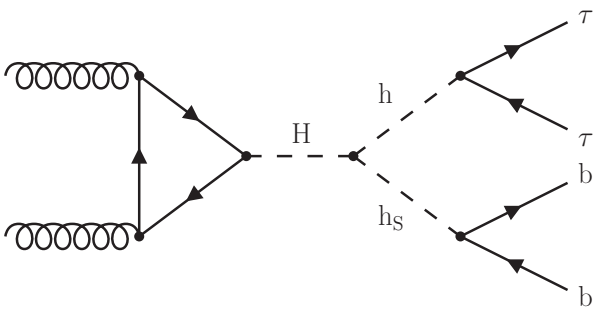

Figure 1. Feynman diagram of the $gg \to H \to h(\tau\tau)h_S(bb)$ process.

2 The CMS detector

The central feature of the CMS apparatus is a superconducting solenoid of 6 m internal diameter, providing a magnetic field of 3.8 T. Within the solenoid volume are a silicon pixel and strip tracker, a lead tungstate crystal electromagnetic calorimeter (ECAL), and a brass and scintillator hadron calorimeter (HCAL), each composed of a barrel and two endcap sections. Forward calorimeters extend the pseudorapidity (η) coverage provided by the barrel and endcap detectors. Muons are detected in gas-ionization chambers embedded in the steel flux-return yoke outside the solenoid.

The silicon tracker measures charged particles within the range of $|\eta| < 2.5$. During the LHC data-taking period up to 2017, the silicon tracker consisted of 1440 silicon pixel and 15 148 silicon strip detector modules. From 2017 on, the silicon pixel detector was upgraded to 1856 modules. For nonisolated particles with a transverse momentum of $1 < p_T < 10$ GeV with respect to the beam axis and $|\eta| < 1.4$, the track resolutions are typically 1.5% in p_T and 25–90 (45–150) μm in the transverse (longitudinal) impact parameter [26]. From 2017 on, the transverse impact parameter resolution improved to 20–60 μm when restricted to the same η range as before and 20–75 μm in the increased full η range [27].

The momentum resolution for electrons with $p_T \approx 45$ GeV from $Z \to ee$ decays ranges from 1.7 to 4.5%. It is generally better in the barrel region than in the endcaps, and also depends on the bremsstrahlung energy emitted by the electron traversing the material in front of the ECAL [28].

Muons are measured in the range of $|\eta| < 2.4$, with detection planes made using three technologies: drift tubes, cathode strip chambers, and resistive plate chambers. The relative p_T resolution for muons with $20 < p_T < 100$ GeV is 1.3 to 2.0% in the barrel and better than 6% in the endcaps. In the barrel the relative p_T resolution is better than 10% for muons with p_T up to 1 TeV [29].

In the barrel section of the ECAL, an energy resolution of about 1% is achieved for unconverted or late-converting photons in the tens of GeV energy range. The remaining barrel photons have a resolution of about 1.3% up to $|\eta| = 1$, rising to about 2.5% at $|\eta| = 1.4$. In the endcaps, the resolution of unconverted or late-converting photons is about 2.5%, while the remaining endcap photons have a resolution of 3–4% [30].

JHEP11(2021)057

When combining information from the entire detector, the jet energy resolution amounts typically to 15–20% at 30 GeV, 10% at 100 GeV, and 5% at 1 TeV [31].

Events of interest are selected using a two-tiered trigger system. The first level (L1), composed of custom hardware processors, uses information from the calorimeters and muon detectors to select events at a rate of around 100 kHz within a fixed latency of about 4 μs [32]. The second level, known as the high-level trigger (HLT), consists of a farm of processors running a version of the full event reconstruction software optimized for fast processing, and reduces the event rate to around 1 kHz before data storage [33].

A more detailed description of the CMS detector, together with a definition of the coordinate system used and the relevant kinematic variables, can be found in ref. [34].

3 Event reconstruction

The reconstruction of the proton-proton (pp) collision products is based on the particle-flow (PF) algorithm, as described in ref. [35], combining the available information from all CMS subdetectors to reconstruct individual particle candidates, categorized into electrons, photons, muons, charged and neutral hadrons. The average number of interactions per bunch crossing in the data of the years 2016 (2017 and 2018) used in this search was 23 (32). The fully recorded detector data of a bunch crossing defines an event for further processing. The candidate vertex with the largest value of summed physics-object p_{T}^2 is taken to be the primary vertex (PV) of the event. The physics objects for this purpose are the jets, formed using the anti-k_{T} jet finding algorithm as implemented in the FastJet package [36] with the tracks assigned to the corresponding candidate vertex as inputs, and the associated missing transverse momentum, taken as the negative vector sum of the p_{T} of those jets. Secondary vertices, which are displaced from the PV in the transverse plane are indicative of decays of long lived particles emerging from the PV. Any other collision vertices in the event are associated with additional mostly soft inelastic pp collisions called pileup (PU).

Electron candidates are reconstructed by fitting tracks in the tracker, and then matching the tracks to clusters in the ECAL [28, 37]. To increase their purity, reconstructed electrons are required to pass a multivariate electron identification discriminant, which combines information on track quality, shower shape, and kinematic quantities. For this analysis, a working point with an identification efficiency of 90% is used, for a rate of jets misidentified as electrons of ≈1%.

Muons in the event are reconstructed by performing a simultaneous track fit to hits in the tracker and in the muon detectors [29, 38]. The presence of hits in the muon detectors already leads to a strong suppression of particles misidentified as muons. Additional identification requirements on the track fit quality and the compatibility of individual track segments with the fitted track reduce the misidentification rate further. For this analysis, muon identification requirements with an efficiency of ≈99% are chosen.

The contributions from backgrounds to the electron and muon selections are further reduced by requiring the corresponding lepton to be isolated from any hadronic activity in

JHEP11(2021)057

the detector. This property is quantified by an isolation variable

$$I_{\text{rel}}^{\text{e}(\mu)} = \frac{1}{p_{\text{T}}^{\text{e}(\mu)}} \left(\sum p_{\text{T}}^{\text{charged}} + \max \left(0, \sum E_{\text{T}}^{\text{neutral}} + \sum E_{\text{T}}^{\gamma} - p_{\text{T}}^{\text{PU}} \right) \right), \tag{3.1}$$

where $p_{\text{T}}^{\text{e}(\mu)}$ corresponds to the electron or muon p_{T} and $\sum p_{\text{T}}^{\text{charged}}$, $\sum E_{\text{T}}^{\text{neutral}}$, and $\sum E_{\text{T}}^{\gamma}$ to the p_{T} (transverse energy E_{T}) sum of all charged particles, neutral hadrons, and photons, in a predefined cone of radius $\Delta R = \sqrt{(\Delta\eta)^2 + (\Delta\phi)^2}$ around the lepton direction at the PV, where $\Delta\phi$ (measured in radians) and $\Delta\eta$ correspond to the angular distances of the particle to the lepton in the azimuthal angle ϕ and η directions, respectively [28, 29]. The chosen cone sizes are $\Delta R < 0.3$ for electrons and 0.4 for muons. The lepton itself is excluded from the calculation. To mitigate any distortions from PU, only those charged particles whose tracks are associated with the PV are taken into account. Since for neutral hadrons and photons an unambiguous association to the PV or PU is not possible, an estimate of the contribution from PU (p_{T}^{PU}) is subtracted from the sum of $\sum E_{\text{T}}^{\text{neutral}}$ and $\sum E_{\text{T}}^{\gamma}$. This estimation is obtained from tracks not associated to the PV in the case of I_{rel}^{μ} and from the mean energy flow per unit area in the case of $I_{\text{rel}}^{\text{e}}$. In the case of negative values, the results are set to zero.

For further characterization of an event, all reconstructed PF objects are used to form jets using the anti-k_{T} jet finding algorithm with a distance parameter of 0.4. To identify jets resulting from the hadronization of b quarks (b jets) the DeepJet algorithm is used as described in refs. [39, 40]. In this analysis a working point of this algorithm is chosen that corresponds to an expected b jet identification efficiency of ≈80% for an expected misidentification rate for jets originating from light quarks and gluons (c quarks) of 1% (15%) [41]. Jets with $p_{\text{T}} > 30\,\text{GeV}$ and $|\eta| < 4.7$ and b jets with $p_{\text{T}} > 20\,\text{GeV}$ and $|\eta| < 2.4\,(2.5)$ are used, where the value in parentheses corresponds to the selection after the upgrade of the silicon pixel detector from 2017 on.

Jets are also used as seeds for the reconstruction of hadronic τ decays (τ_{h}). This is done by further exploiting the substructure of the jets, using the hadrons-plus-strips algorithm, as described in ref. [42]. For the analysis, the decays into one or three charged hadrons with up to two neutral pions with $p_{\text{T}} > 2.5\,\text{GeV}$ are used. The neutral pions are reconstructed as strips with dynamic size in η-ϕ from reconstructed electrons and photons contained in the seeding jet, where the strip size varies as a function of the p_{T} of the electron or photon candidate. The τ_{h} decay mode is then obtained by combining the charged hadrons with the strips. To distinguish the τ_{h} decays from jets originating from the hadronization of quarks or gluons, and from electrons, or muons, the DeepTau algorithm is used, as described in ref. [43]. This algorithm exploits the information of the reconstructed event record, comprising tracking, impact parameter, and ECAL and HCAL cluster information; the kinematic and object identification properties of the PF candidates in the vicinity of the τ_{h} candidate and the τ_{h} candidate itself; and several characterizing quantities of the whole event. It results in a multiclassification output y_{α}^{DT} ($\alpha = \tau, \text{jet}, \text{e}, \mu$) equivalent to a Bayesian probability of the τ_{h} candidate to originate from a genuine tau, the hadronization of a quark or gluon, an isolated electron, or an isolated muon. From this output three

JHEP11(2021)057

discriminators are built according to

$$D_\alpha = \frac{y_\tau^{\mathrm{DT}}}{y_\tau^{\mathrm{DT}} + y_\alpha^{\mathrm{DT}}}, \quad \alpha = \mathrm{jet},\, \mathrm{e},\, \mu. \tag{3.2}$$

For this analysis, a working point of D_{jet} with a genuine τ_{h} identification efficiency of 70% for a misidentification rate of 0.43% is chosen. For D_{e} and D_μ, depending on the $\tau\tau$ final state, different working points with efficiencies of 80% and >99% and misidentification rates between 0.03% and 2.60% are chosen, respectively. It should be noted that the misidentification rate of D_{jet} strongly depends on the p_{T} and quark flavor of the misidentified jet, which is why this number should be viewed as an approximate estimate.

The pileup-per-particle identification algorithm [44] is applied to reduce the PU dependence of the $\vec{p}_{\mathrm{T}}^{\,\mathrm{miss}}$ observable, which is computed as the negative vectorial p_{T} sum of the PF candidates, weighted by their probability to originate from the PV [45]. Its magnitude is referred to as $p_{\mathrm{T}}^{\mathrm{miss}}$. It is used for the estimation of the invariant mass of the two tau leptons before their decay, as discussed in section 5.

4 Data model

The selection given in section 5 targets the reconstruction of a pair of tau leptons originating from h with a mass of $m_{\tau\tau} = 125\,\mathrm{GeV}$ and a pair of b quarks originating from $\mathrm{h_S}$ with a mass varying between 60 and 2800 GeV. For the τ pair the $\mathrm{e}\tau_{\mathrm{h}}$, $\mu\tau_{\mathrm{h}}$ and $\tau_{\mathrm{h}}\tau_{\mathrm{h}}$ final states are used. The contribution of the $\mathrm{e}\mu$ final state to the sensitivity of the search has been found to be negligible, which can be understood from the low $\tau\tau$ branching fraction and the overwhelmingly large background from t quark pair production ($\mathrm{t\bar{t}}$). In the $\mathrm{e}\tau_{\mathrm{h}}$ and $\mu\tau_{\mathrm{h}}$ final states, the most abundant source of background after the selection is $\mathrm{t\bar{t}}$ that can easily result in a signature with genuine leptons and b quarks. After selection the expected fraction of $\mathrm{t\bar{t}}$ events in these final states is ≈70%. In the $\tau_{\mathrm{h}}\tau_{\mathrm{h}}$ final state, events containing purely quantum chromodynamics (QCD) induced gluon and quark jets, referred to as QCD multijet production in the following, and the decay of Z bosons into tau leptons form the largest background sources with ≈35% each.

All SM background sources of relevance for this analysis are listed in table 1. For the background modeling, three different methods are used depending on the interpreted signature after reconstruction: (i) $\tau\tau$ events are obtained from the τ-embedding method, discussed in section 4.1; (ii) events with jets misidentified as τ_{h} (jet → τ_{h}) are obtained from the F_{F}-method, discussed in section 4.2; (iii) all other background events and the signal events are obtained from full event simulation, discussed in section 4.3.

4.1 The τ-embedding method

For all events in which the decay of a Z or two W bosons results in two genuine tau leptons, the τ-embedding method, as described in ref. [46], is used. For this purpose, $\mu\mu$ events are selected in data. All energy deposits of the muons are removed from the event record and replaced by simulated tau lepton decays with the same kinematic properties as the selected muons. In this way the method relies only on the simulation of the well-understood tau

JHEP11(2021)057

Background process	Final state signature	Estimation method τ-emb.	F_F	Sim.
Z	ττ	✓	—	—
	Jet → τ_h	—	✓	—
	$\ell\ell$	—	—	✓
$t\bar{t}$	ττ + X	✓	—	—
	Jet → τ_h	—	✓	—
	$\ell + X$	—	—	✓
Diboson+single t	ττ + X	✓	—	—
	Jet → τ_h	—	✓	—
	$\ell + X$	—	—	✓
W+jets	Jet → τ_h	—	✓	—
QCD multijet	Jet → τ_h	—	✓	—
Single h	ττ	—	—	✓
	bb	—	—	✓

$\ell = e, \mu$

Table 1. Background processes contributing to the event selection, as given in section 5. The symbol ℓ corresponds to an electron or muon. The second column refers to the experimental signature in the analysis, the last three columns indicate the estimation methods used to model each corresponding signature, as described in sections 4.1–4.3.

lepton decay and its energy deposits in the detector, while all other parts of the event, such as the reconstructed jets, their identification as originating from the PV, the identification of b jets, or the non-τ related parts of p_T^{miss}, are obtained from data. This obviates the need to simulate complicated processes, such as parton showering, hadronization, underlying event, and event pileup, which are difficult to model in simulation, and results in an improved description of the data compared to the simulation of the full process. In turn, several simulation-to-data corrections, as detailed in section 4.4, are not needed.

The selected muons predominantly originate from Z boson decays; however, contributions from other processes resulting in two genuine tau leptons, like $t\bar{t}$ or diboson production, are also covered by this model, where throughout the text diboson refers to any combination of two W or Z bosons. A detailed discussion of the selection of the original μμ events, the exact procedure itself, its range of validity, and related uncertainties can be found in ref. [46]. For a selection with at least one jet identified as a b jet in the event, as described in section 5, 84% of the μμ events selected for the τ-embedding method are expected to originate from Z boson decays, 14% from $t\bar{t}$, and ≈2% from diboson production.

JHEP11(2021)057

4.2 The F_F-method

The main contributing processes to jet $\to \tau_h$ events are QCD multijet production, W bosons in association with jets (W+jets), and $t\bar{t}$. These events are estimated using the F_F-method, as described in refs. [22, 47]. For this purpose the complete kinematic phase space is split into the disjoint signal region (SR), application region (AR), and determination regions (DR^i). The SR and the AR differ only in the working point chosen for the identification of the τ_h candidate, where for the AR a looser working point is chosen and the events from the SR are excluded. Three independent extrapolation factors F_F^i are derived for QCD multijet, W+jets production, and $t\bar{t}$ in three dedicated DR^i, defined to enrich each corresponding process. The F_F^i are then used to estimate the yields N_{SR} and kinematic properties of the combination of these backgrounds in the SR from the number of events N_{AR} in the AR according to

$$N_{SR} = \left(\sum_i w_i F_F^i\right) N_{AR} \qquad i = \text{QCD, W+jets, } t\bar{t}. \tag{4.1}$$

For this purpose the F_F^i are combined into a weighted sum, using the simulation-based estimation of the fractions w_i of each process in the AR.

For the estimate of F_F^{QCD}, the charges of the two selected τ decay products are required to be of same sign. For the estimation of F_F^{W+jets}, a b jet veto and a high transverse mass of the lepton-p_T^{miss} system are required. The estimation of $F_F^{t\bar{t}}$ is obtained from simulation, with a selection of more than two jets, at least one b jet, and more than two leptons in an event. Each F_F^i is derived on an event-by-event basis, as a function of the p_T of the τ_h candidate, the p_T of the second τ decay in the event, and the mass of the visible $\tau\tau$ decay products. All other processes but the enriched background process are estimated from the τ-embedding method or simulation and subtracted for this purpose. Each F_F^i is further subject to a number of nonclosure corrections derived from control regions in data to take sub-leading dependencies of the F_F^i into account.

4.3 Simulation

In the $\tau_h\tau_h$ final state, the τ-embedding and F_F-methods cover ≈95% of all expected background events. In the $e\tau_h$ and $\mu\tau_h$ final states the fractions of expected background events described by these two methods are ≈42%, each. All remaining events originate from processes like Z boson, $t\bar{t}$, or diboson production, where at least one decay of a vector boson into an electron or muon is not covered by any of the two methods. These and the signal events are modeled using the simulation of the full processes.

The production of Z bosons in the ee and $\mu\mu$ final states is simulated at leading-order (LO) precision in the coupling strength α_S, using the MadGraph5_aMC@NLO 2.2.2 (2.4.2) event generator [48, 49] for the simulation of the data taken in 2016 (2017 and 2018). To increase the number of simulated events in regions of high signal purity, supplementary samples are generated with up to four outgoing partons in the hard interaction. For diboson production MadGraph5_aMC@NLO is used at next-to-LO (NLO) precision in α_S. For $t\bar{t}$ and single t quark production samples are generated at NLO precision using

JHEP11(2021)057

POWHEG 2.0 [50–55]. The kinematic properties of single h production are simulated at NLO precision using POWHEG separately for the production via gluon fusion, vector boson fusion, or in association with a Z boson, W boson, or a top quark pair. For this purpose h is assumed to behave as expected from the SM.

When compared to data, Z boson, $\mathrm{t\bar{t}}$, and single t quark events in the tW channel are normalized to their cross sections at next-to-NLO precision in α_S [56–58]. Single t quark production in the t-channel and diboson events are normalized to their cross sections at NLO precision in α_S or higher [58–60].

The signal process $\mathrm{H} \to \mathrm{h}\mathrm{h}_S$ is generated using MadGraph5_aMC@NLO at LO precision. The analysis is restricted to H production via gluon fusion, which is expected to be dominant, e.g., in the NMSSM. Due to the two unknown masses involved in the decay, a two-dimensional grid of signal mass pairs is generated, resulting in 420 mass pairs spanning from 240 to 3000 GeV in m_H and 60 to 2800 GeV in m_{h_S}, only taking pairs with $m_{h_S} + 125\,\mathrm{GeV} \leq m_H$ into account.

For the generation of all signal and background processes, the NNPDF3.0 [61] (NNPDF3.1 [62]) parton distribution functions are used for the simulation of the data taken in 2016 (2017 and 2018). The description of the underlying event is parameterized according to the CUETP8M1 [63] and CP5 [64] tunes. Parton showering and hadronization, as well as the τ lepton decays, are modeled using the PYTHIA 8.230 event generator [65]. For all simulated events, additional inclusive inelastic pp collisions generated with PYTHIA are added according to the expected PU profile in data to take the effect of the observed PU into account. All events generated are passed through a GEANT4-based [66] simulation of the CMS detector and reconstructed using the same version of the CMS event reconstruction software as used for the data.

4.4 Corrections and control of the model

The capability of the model to describe the data is monitored in various control regions orthogonal to the signal and background classes defined in section 5, and corrections and corresponding uncertainties are derived where necessary.

The following corrections equally apply to simulated and τ-embedded events, where the τ decay is also simulated. Since the simulation part for τ-embedded events happens under detector conditions, which are different from the case of fully simulated events, corrections and related uncertainties may differ, as detailed in ref. [46]. Corrections are derived for residual differences between data and simulation in the efficiency of the selected triggers, the electron and muon tracking efficiency, and in the efficiency of the identification and isolation requirements for electrons and muons. These corrections are obtained in bins of p_T and η of the corresponding lepton, using the "tag-and-probe" method, as described in ref. [67], with $\mathrm{Z} \to \mathrm{ee}$ and $\mathrm{Z} \to \mu\mu$ events. They usually amount to not more than a few percent.

In a similar way, corrections are obtained for the efficiency of triggering on the τ_h decay signature and for the τ_h identification efficiency, following procedures as described in ref. [42]. The latter are derived as a function of the p_T of the τ_h in four bins below 40 GeV and one bin above. For $p_T(\tau_h) > 40\,\mathrm{GeV}$, a correction is also derived for each τ_h decay mode individually, which is used only in the $\tau_h\tau_h$ final state. Corrections to the

JHEP11(2021)057

energy scale of the τ_h decays and of electrons misidentified as τ_h are derived for each year of data-taking and each τ_h decay mode individually, from likelihood scans of discriminating observables, like the mass of the visible decay products of the τ_h candidate, as detailed in ref. [42]. For muons misidentified as τ_h this effect has been observed to be negligible. For the trigger efficiency the correction is obtained from parametric fits to the trigger efficiency as a function of p_T derived for each corresponding sample and data.

The following corrections only apply to fully simulated events. During the 2016 and 2017 data-taking, a gradual shift in the timing of the inputs of the ECAL L1 trigger in the region at $|\eta| > 2.0$ caused a specific trigger inefficiency. For events containing an electron (a jet) with p_T larger than $\approx$50 ($\approx$100) GeV, in the region of $2.5 < |\eta| < 3.0$ the efficiency loss is 10–20%, depending on p_T, η, and time. Corresponding corrections have been derived from data and applied to the simulation.

The jet energy is corrected to the expected response at the stable hadron level, using corrections measured in bins of the jet p_T and η, as described in ref. [31]. These corrections are usually not larger than 10–15%. Residual data-to-simulation corrections are applied to the simulated event samples. They usually range between subpercent level at high jet p_T in the central part of the detector to a few percent in the forward region. A correction is applied to the direction and magnitude of $\vec{p}_T^{\,\text{miss}}$ based on differences between estimates of the hadronic recoil in $Z \to \mu\mu$ events in data and simulation, as described in ref. [45]. This correction is applied to the simulated Z boson, single h, and signal events, where a hadronic recoil against a single particle is well defined.

The efficiencies for genuine and misidentified b jets to pass the working points of the b jet identification discriminator, as given in section 3, are determined from data, using $t\bar{t}$ events for genuine b jets and Z boson production in association with jets originating from light quarks or gluons. Data-to-simulation corrections are obtained for these efficiencies and used to correct the number of b jets in the simulation, as described in ref. [39].

Data-to-simulation corrections are further applied to $Z \to ee$ ($Z \to \mu\mu$) events in the $e\tau_h$ ($\mu\tau_h$) and $\tau_h\tau_h$ final states in which an electron (muon) is reconstructed as a τ_h candidate, to account for residual differences in the $e(\mu) \to \tau_h$ misidentification rate between data and simulation. Deficiencies in the modeling of Z boson events in the ee, $\mu\mu$ final states, due to the use of a LO simulation, are corrected for by reweighting the simulated $Z \to \mu\mu$ events to data in bins of $p_T^{\mu\mu}$ and $m_{\mu\mu}$. In addition all simulated $t\bar{t}$ events are weighted to better match the top quark p_T distribution, as observed in data [68].

The overall normalization of all backgrounds is constrained by dedicated event categories, obtained from neural network (NN) multiclassification, as described in section 5. After the event selection and prior to the event classification, i.e., still at an inclusive state of the analysis, the marginal distributions and pairwise correlations, including self-correlations, of all input features to the NNs used for event classification are subject to extensive scrutiny. This is done exploiting goodness-of-fit tests, based on a saturated likelihood model [69] including all systematic uncertainties of the model and their correlations, as used for the signal extraction. This guarantees a good understanding of the input space to the NNs and the input distributions used for the statistical inference of the signal contribution.

JHEP11(2021)057

Final state	Electron/Muon	τ_h
$e\tau_h$	$p_T > 25\,(26,\,28,\,33)$ GeV	$p_T > 35\,(30)$ GeV
	$\lvert\eta\rvert < 2.1$	$\lvert\eta\rvert < 2.3$
	$I^e_{rel} < 0.15$	D_{jet} (70%), D_e (0.05%), D_μ (0.13%)
$\mu\tau_h$	$p_T > 20\,(23,\,25)$ GeV	$p_T > 35\,(30)$ GeV
	$\lvert\eta\rvert < 2.1$	$\lvert\eta\rvert < 2.3$
	$I^\mu_{rel} < 0.15$	D_{jet} (70%), D_e (2.60%), D_μ (0.03%)
$\tau_h\tau_h$	—	$p_T > 40$ GeV
		$\lvert\eta\rvert < 2.1$
		D_{jet} (70%), D_e (2.60%), D_μ (0.13%)

Table 2. Offline requirements applied to electrons, muons, and τ_h candidates used for the selection of the τ pair. The p_T values in parentheses correspond to events selected by a single-electron or single-muon trigger. These requirements depend on the year of data-taking. For D_{jet} the efficiency and for $D_{e(\mu)}$ the misidentification rates for the chosen working points are given in parentheses. A detailed discussion is given in the text.

5 Event selection and classification

5.1 Event selection

The L1 trigger decision is based on the identification of high-p_T electrons or muons, reconstructed from a fast readout of the ECAL and muon detectors. A positive L1 trigger decision initiates the further reconstruction of the given event at the HLT. In the HLT step, the selection is based on the presence of a single electron or muon, an $e\tau_h$ or $\mu\tau_h$ pair, or a $\tau_h\tau_h$ pair in the event. The addition of the single-electron or single-muon requirement to the list of triggers via a logical OR condition increases the overall acceptance of the online selection. In the offline selection further requirements on the p_T, η, $I^{e(\mu)}_{rel}$, and the D_α discriminators are applied in addition to the object identification requirements described in section 3, as summarized in table 2.

In the $e\tau_h$ ($\mu\tau_h$) final state, an electron (muon) with at least 25 (20) GeV is required, if an event was selected by a trigger based on the presence of the $e\tau_h$ ($\mu\tau_h$) pair. If the event was selected by a single-electron trigger, the p_T requirement on the electron is increased to 26–33 GeV depending on the data-taking period, to ensure a sufficiently high efficiency of the HLT selection. For muons, the p_T requirement is increased to 23 (25) GeV for 2016 (2017 or 2018), if selected by a single-muon trigger. The electron (muon) is required to be contained in the central detector with $\lvert\eta\rvert < 2.1$, and to be isolated from any hadronic activity according to $I^{e(\mu)}_{rel} < 0.15$. The τ_h candidate is required to have $\lvert\eta\rvert < 2.3$ and $p_T > 35$ GeV if selected by an $e\tau_h$ ($\mu\tau_h$) pair trigger, or $p_T > 30$ GeV if selected by a single-electron (single-muon) trigger. In the $\tau_h\tau_h$ final state, both τ_h candidates are required to have $\lvert\eta\rvert < 2.1$ and $p_T > 40$ GeV. The working points of the DeepTau discriminants, as

JHEP11(2021)057

described in section 3, are chosen depending on the final state. Events with additional leptons fulfilling looser selection criteria are discarded to avoid the assignment of single events to more than one final state.

The selected τ decay candidates are required to be of opposite charge and to be separated by more than $\Delta R = 0.5$ in the η-ϕ plane. The closest distance of their tracks to the PV is required to be $d_z < 0.2\,\text{cm}$ along the beam axis. For electrons and muons, an additional requirement of $d_{xy} < 0.045\,\text{cm}$ in the transverse plane is applied. In rare cases in which an extra τ_h candidate fulfilling all selection requirements is found, the candidate with the higher score of D_{jet} is chosen.

In addition to the tau lepton pair, at least one b jet fulfilling the selection criteria, as described in section 3, is required. Events that contain only one b jet and no other jet are removed from the analysis. If more than two b jets exist, the pair is built from those that are leading in p_T. If only one b jet exists the b pair is built using the b jet and the jet with its highest b jet score of the DeepJet classifier. The energies of the jets used for the b pair are corrected using the multivariate energy-momentum regression described in ref. [70].

This analysis selection is optimized for the reconstruction of events where the h and h_S decay products are spatially resolved. Boosted topologies, which can occur in parts of the explored mass ranges, are not specifically targeted.

5.2 Event classification

All events retained by the selection described above are further sorted into five categories. One for signal, the other four are enriched with different backgrounds. This is done separately for each of the three final states and each of the three data-taking periods resulting in 45 categories. The background-enriched categories are used to further constrain systematic uncertainties in the background estimates during the statistical inference of the signal contribution. This categorization is based on NN multiclassification exploiting fully connected feed-forward NNs with two hidden layers of 200 nodes each, and five output nodes implemented in the software package TensorFlow [71]. The first four output nodes used to enrich the backgrounds comprise the following events: (i) events containing genuine τ pairs (labeled "$\tau\tau$"); (ii) events with quark or gluon induced jets misidentified as τ_h (labeled "jet $\to \tau_h$"); (iii) top quark pair events where the intermediate W bosons decay into any combination of electrons and muons, or into a single τ and an electron or muon (not included in (i) or (ii); labeled as "tt"); (iv) events from remaining background processes that are of minor importance for the analysis and not yet included in any of the previous classes (labeled as "misc"). The processes in (iv) comprise diboson production, single t quark production, Z boson decays to electrons or muons, and single h production. For single h production, rates and branching fractions as predicted by the SM are assumed. Event classes (i) and (ii) are defined by final state or experimental signature of the contained events rather than explicit underlying physics processes. They are complemented by event classes (iii) and (iv) to characterize all background processes, which are of relevance for the analysis. The fifth event class, associated with the fith output node, contains the $H \to h(\tau\tau)h_S(bb)$ signal events (labeled as "signal"). This choice of event classes closely resembles the data model described in section 4.

JHEP11(2021)057

For each node in the hidden layers, the hyperbolic tangent is chosen as the activation function. The activation function for the output layer is chosen to be the softmax function allowing for a Bayesian conditional probability interpretation $y_i^{(k)}$ of an event k to be associated to an event class i, given its input features $\vec{x}^{(k)}$ to the NN. The highest value of $y_i^{(k)}$, $\max(y_i^{(k)})$, defines which class the event is associated with and will define the discriminator for the statistical inference of the signal contribution. All other outputs $y_j^{(k)}$, $j \neq i$ are discarded from any further consideration so that any event is used only once for the statistical inference of the signal.

In the $e\tau_h$ and $\mu\tau_h$ final states, the input space to the NNs is spanned by 20 features $\vec{x}$ of an event including p_T of the τ candidates and the jets forming the b quark pair; the mass and p_T estimates of the τ pair, b quark pair, and $\tau\tau bb$ system; the number of (b) jets; and further kinematic properties of the selected jets. For this purpose, a likelihood-based estimate of the $\tau\tau$ mass before decay [72] and a kinematic fit to the $\tau\tau bb$ system for each given m_H and m_{h_S} hypothesis, similar to the approach described in ref. [73], are used. In the $\tau_h\tau_h$ final state these features are complemented by the masses of the two jets used for the b quark pair system and their associated output values of the DeepJet algorithm, to allow for a better discrimination of genuine b jets from light quark or gluon induced jets. All input features have been selected from a superset of variables describing the properties of the event exploiting a ranking of individual features and pairwise correlations of features, as described in ref. [74].

Since the kinematic properties of the signal strongly vary across the probed ranges of m_H and m_{h_S} a total of 68 NNs per final state are used for classification, which within each final state only differ by the kinematic properties of the signal that are used for training. For this purpose, adjacent sets of points in m_{h_S} and m_H are combined into single signal classes. Up to four points in m_{h_S} are combined for single points in m_H, for $m_H \leq 1000\,\text{GeV}$. Beyond $m_H = 1000\,\text{GeV}$, all remaining points in m_H and up to nine points in m_{h_S} are combined. The concrete grouping is a tradeoff between sensitivity and computational feasibility. Though it reduces the use of the invariant mass of the reconstructed b quark pair (m_{bb}) for the NN decision this grouping of mass points has only a small effect on the overall NN performance in separating signal from background, which can be understood by the following means: (i) correlated information, like the m_H estimate and the χ^2 of the kinematic fit are used, in addition to m_{bb}; (ii) the fact that m_{bb} is a peaking distribution for signal while not for background is still fully exploited by the NN; (iii) for $m_H > 1000\,\text{GeV}$ the p_T of the jets forming the b quark pair gains importance. Differences of the input features depending on the year of data-taking are taken into account by a conditional training using a one-hot encoding of the data-taking year in the NN training, such that the correct year of data taking obtains the value 1, while all other data-taking years obtain the value 0.

The parameters to be optimized during training are the weights ($\{w_a\}$) and biases ($\{b_b\}$) of the NN output functions y_i. Before training the weights are initialized with random numbers using the Glorot initialization technique [75] with values drawn from a uniform distribution. The biases are initialized with zero. The trainings are then performed using randomly sampled batches of $N = 30$ events per event class, drawn from the training

JHEP11(2021)057

datasets using a balanced batch approach [76]. This approach has shown improved convergence properties on training samples with highly imbalanced lengths. The classification task is encoded in the NN loss function, chosen as the cross entropy

$$L\left(\{y_i^{(k)}\},\{y_j'^{(k)}\}\right) = -\sum_{k=1}^{N} y_j'^{(k)} \log\left(y_i^{(k)}(\{w_a\},\{b_b\},\{\vec{x}^{(k)}\})\right) ; \qquad y_j'^{(k)} = \delta_{ij}, \tag{5.1}$$

which is to be minimized during the NN trainings. In eq. (5.1), k runs over the events in the batch, on which L is evaluated. The NN prediction for event k to belong to category i is given by $y_i^{(k)}$. The function $y_j'^{(k)}$ encodes the prior knowledge of the training. It is 1 if class i of event k coincides with the true event class j, and 0 otherwise. The $y_i^{(k)}$ depend on the weights, biases, and input features $\{\vec{x}^{(k)}\}$ of event k to the NN. The batch definition guarantees that each true event class enters the training with equal weight in the evaluation of L, i.e., without prevalence. Within the misc event class all contained processes are normalized according to their expected rates with respect to each other. On each batch a gradient step is applied, defined by the partial derivatives of L in each weight, w_a, and bias, b_b, using the Adam minimization algorithm [77], with a constant multiplicative learning rate of 10^{-4}. To guarantee statistical independence, those events that are used for training are not used for any other step of the analysis.

The performance of the NNs during training is monitored by evaluating L on a validation subset that contains a fraction of 25% of randomly chosen events from the training sample, which are excluded from the gradient computation. The training is stopped if the evaluation of L on the validation dataset does not indicate any further decrease for a sequence of 50 epochs, where an epoch is defined by 1000 (100) batches in the $\mathrm{e}\tau_\mathrm{h}/\mu\tau_\mathrm{h}$ ($\tau_\mathrm{h}\tau_\mathrm{h}$) final state. The NNs used for the analysis are then defined by the weights and biases of the epoch with the minimal value of L on the validation sample.

To improve the generalization property of the NNs, two regularization techniques are introduced. Firstly, after each hidden layer a layer with a dropout probability of 30% is added. Secondly, the weights of the NNs are subject to an L2 (Tikhonov) regularization [78] with a regularization factor of 10^{-5}.

After training, a very good separation between the background events and the signal events is achieved, with a purity and classification sensitivity for the correct signal class of typically more than 80%.

6 Systematic uncertainties

The uncertainty model used for the analysis comprises theoretical uncertainties, experimental uncertainties, and uncertainties due to the limited population of template distributions for the background model used for the statistical inference of the signal, as described in section 7. The last group of uncertainties is incorporated for each bin of each corresponding template individually following the approach proposed in ref. [79]. For this analysis, where the signal is expected to be concentrated to a few bins with low background expectation, these uncertainties can often range among those with the largest impact on the signal significance. All other uncertainties lead to correlated changes across bins either in the form

JHEP11(2021)057

of normalization changes or as general nontrivial shape-altering variations. Depending on the way they are derived, correlations may also arise across years, samples, or individual uncertainties.

The following uncertainties related to the level of control of the reconstruction of electrons, muons, and τ_h candidates after selection apply to simulated and τ-embedded events. Unless stated otherwise they correspond to the uncertainties of the corrections described in section 4.4 and are partially correlated across τ-embedded and simulated events.

- Uncertainties in the identification efficiency of electrons and muons amount to 2%, correlated across all years. Since no significant dependence on the p_T or η of each corresponding lepton is observed these uncertainties are introduced as normalization uncertainties.

- With a similar reasoning, uncertainties in the electron and muon trigger efficiencies are also introduced as normalization uncertainties. They amount to 2% each. Due to differences in the trigger leg definitions they are treated as uncorrelated for single-lepton and two-object triggers. This may result in shape-altering effects in the overall model, since both triggers act on different regions in lepton p_T.

- For fully simulated events an uncertainty in the electron energy scale is derived from the calibration of ECAL crystals, and applied on an event-by-event basis [28]. For τ-embedded events uncertainties of 0.50–1.25%, split by the ECAL barrel and endcap regions, are derived for the corrections described in section 4.4. Due to the different ways the uncertainties are determined and differences in detector conditions they are treated as uncorrelated across simulated and τ-embedded events. They lead to shape-altering variations and are treated as correlated across years. The muon momentum (p_μ) is very precisely known [38]. A variation within the given uncertainties, depending on the muon η and p_T has been checked to have no influence on the analysis.

- Uncertainties in the τ_h-identification range between 3 and 5% in bins of τ_h p_T. Due to the nature of how they are derived these uncertainties are statistically dominated and therefore treated as uncorrelated across decay modes, p_T bins, and years. The same is true for the uncertainties in the τ_h-energy scale, which range from 0.2 to 1.1%, depending on the p_T and the decay mode of the τ_h. For the energy scale of electrons misidentified as τ_h candidates, extra corrections are derived depending on the τ_h p_T and decay mode. Their uncertainties range from 1.0 to 2.5%. Concerning correlations the same statements apply as for the τ_h-energy scale. All uncertainties discussed here for the τ_h identification and energy scale lead to shape-altering variations. A generous variation of the momentum scale of muons misidentified as τ_h has been checked to have a marginal effect on the analysis.

- Uncertainties in the τ_h trigger efficiency are 5–10%, depending on the p_T of the τ_h. They are obtained from parametric fits to data and simulation, and lead to shape-altering effects. They are treated as uncorrelated across triggers and years.

Two further sources of uncertainty are considered for τ-embedded events [46]:

JHEP11(2021)057

- A 4% normalization uncertainty accounts for the level of control in the efficiency of the $\mu\mu$ selection in data, which is unfolded during the τ-embedding procedure. The dominant part of this uncertainty originates from the trigger used for selection and is treated as uncorrelated across years.

- Another shape and normalization-altering uncertainty in the yield of $t\bar{t} \to \mu\mu + X$ decays, which are part of the τ-embedded event samples, ranges between subpercent and 10%, depending on the event composition of the model. For this uncertainty, the number and shape of $t\bar{t}$ events contained in the τ-embedded event samples are estimated from simulation, for which the corresponding decay has been selected at the parton level. This estimate is then varied by $\pm 10\%$.

For fully simulated events the following additional uncertainties apply:

- Uncertainties in the $e(\mu) \to \tau_h$ misidentification rate amount to 40% for electrons and range from 10 to 70% for muons. The relatively large size of these uncertainties originates from the rareness of these cases in the control regions that are used to measure these rates. They only apply to simulated $Z \to ee\,(\mu\mu)$ events, which are of marginal importance for the analysis. The impact on the overall background yield is below the 1% level both in the $e\tau_h$ and $\mu\tau_h$ final states. The same is true for the uncertainty in the reweighting in the Z boson mass and p_T, discussed in section 4.4, which ranges from 10 to 20%.

- Uncertainties in the energy calibration and resolution of jets are applied with different correlations depending on their sources, comprising statistical limitations of the measurements used for calibration, the time-dependence of the energy measurements in data due to detector aging, and nonclosure corrections introduced to cover residual differences between simulation and data [31]. They range between subpercent level and $\mathcal{O}(10\%)$, depending on the kinematic properties of the jets in the event. Similar uncertainties are applied for the identification rates for b jets and for the misidentification rates for light quark or gluon induced jets, which are of a similar range each [39, 40].

- Depending on the process in consideration, two independent uncertainties in p_T^{miss} are applied. For processes that are subject to recoil corrections, i.e., Z boson production, h production, or signal, uncertainties in the calibration and resolution of the hadronic recoil are applied, ranging from 1 to 5%. For all other processes an uncertainty in p_T^{miss} is derived from the amount of unclustered energy in the event [45].

- A normalization uncertainty due to the timing shift of the inputs of the ECAL L1 trigger described in section 4.4 amounts to 2–3%.

- A shape-altering uncertainty is derived in the reweighting of the top quark p_T described in section 4.4 by applying the correction with twice the required magnitude, thus overcorrecting, or not applying it at all. This uncertainty has only a very small effect on the final discriminator.

JHEP11(2021)057

- The integrated luminosity is measured for each year of data-taking individually following procedures, as described in ref. [80]. The luminosity measurements are known to a precision of 2.3 (2.5)% for 2017 [81] (2016 [82] and 2018 [83]). The corresponding normalization uncertainties comprise parts that are correlated and parts that are uncorrelated across the years.

- Uncertainties in the predictions of the normalizations of all simulated processes amount to 6% for $\mathrm{t\bar{t}}$ [57, 58], 5% for diboson and single t production [58–60], 2% for Z boson production [56], and 1.3–3.9% for the SM Higgs boson production rates used for h production, depending on the production mechanism [52, 55, 84–86]. All these uncertainties are correlated across years.

- Since the search is not conducted within any particular model, no uncertainties on the production cross section or branching fractions of the signal need to be taken into account. Uncertainties in the signal acceptance are obtained from variations of the factorization and renormalization scales, as well as from sampling all relevant parameters for the estimation of the parton density distributions within their corresponding uncertainties, following procedures as outlined in [87]. The changes in acceptance due to the scale variations are observed to be less than 10%. They are shape altering, depending on the h and $\mathrm{h_S}$ p_{T}. The acceptance variations due to the sampling of the parton density distributions amount to normalization changes of 18%. Both uncertainties are correlated across years.

For the F_{F}-method the following uncertainties apply:

- The F_{F}^{i} and their corrections are subject to statistical fluctuations in each corresponding DR^{i}. The corresponding uncertainties are split into a normalization and a shape-altering part and propagated into the final discriminator. They usually range between 3–5% and are treated as uncorrelated across the kinematic and topological bins they are derived in.

- Additional uncertainties are applied to cover corrections for non-closure effects and extrapolation factors, varying from a few percent to $\mathcal{O}(10\%)$, depending on the kinematic properties of the τ_{h} candidate and the topology of the event. These are both normalization and shape-altering uncertainties.

- An additional source of uncertainty concerns the subtraction of processes other than the enriched process in each corresponding DR^{i}. These are subtracted from the data using simulated or τ-embedded events. The combined shape of the events to be removed is varied by 7%, and the measurements are repeated. The impacts of these variations are then propagated to the final discriminator as shape-altering uncertainties.

- An uncertainty in the estimation of the three main background fractions in the AR is estimated from a variation of each individual contribution by 7%, increasing or decreasing the remaining fractions such that the sum of all contributions remains

JHEP11(2021)057

unchanged. The amount of variation is motivated by the uncertainty in the production cross sections and acceptances of the involved processes and the constraint on the process composition that can be clearly obtained from the AR. The effect of this variation is observed to be very small, since usually one of the contributions dominates the event composition in the AR.

Due to their mostly statistical nature and differences across years, all uncertainties related to the F_{F}-method are treated as uncorrelated across years. A summary of all systematic uncertainties that have been discussed in this section is given in table 3.

7 Results

The model used to infer the signal from the data is defined by an extended binned likelihood of the form

$$\mathcal{L} = \prod_i \mathcal{P}(k_i|\mu\, S_i(m_{\mathrm{H}},\, m_{\mathrm{h_S}},\, \{\theta_j\}) + B_i(\{\theta_j\})) \prod_j \mathcal{C}(\hat{\theta}_j|\theta_j), \tag{7.1}$$

where i labels all bins of the distributions of the NN output functions $\max(y_i)$ of each of the five signal and background classes defined in section 5. Split by three $\tau\tau$ final states and three years of data-taking this results in 45 individual input histograms, for each given pair of m_{H} and $m_{\mathrm{h_S}}$. The function $\mathcal{P}(k_i|\mu\, S_i(m_{\mathrm{H}},\, m_{\mathrm{h_S}},\, \{\theta_j\}) + B_i(\{\theta_j\}))$ corresponds to the Poisson density to observe k_i events in bin i for a prediction of S_i signal and a total of B_i background events. The parameter μ is a single scaling parameter of the signal.

Systematic uncertainties are incorporated as penalty terms for additional nuisance parameters $\{\theta_j\}$ in the likelihood, appearing as a product with predefined probability density functions $\mathcal{C}(\hat{\theta}_j|\theta_j)$ to obtain a maximum likelihood estimate $\hat{\theta}_j$ for an assumed true value of θ_j, during the statistical inference of the signal [88].

Sets of input distributions based on the NN classification for $m_{\mathrm{H}} = 500\,\mathrm{GeV}$ and $100 \leq m_{\mathrm{h_S}} < 150\,\mathrm{GeV}$ in the $\mu\tau_{\mathrm{h}}$, $e\tau_{\mathrm{h}}$, and $\tau_{\mathrm{h}}\tau_{\mathrm{h}}$ final states are shown in figures 2–4. For these figures, the data from all three years of data-taking have been combined. To retain the shape of the distributions of the y_i in each category, the histogram bins have been divided by their widths, in the upper panels of each figure. As a Bayesian probability estimate the values of y_i range from 0.2 to 1.0. The lower bound is given by the constraint that each event has to be associated to one of the five event categories. In each event category, the targeted processes are expected to have increasing purity with increasing values of y_i. The points with error bars correspond to the data and the stacked filled histograms to the expectation from the background model. For the signal categories, the expectation for a signal with $\sigma\,\mathcal{B}(\mathrm{H} \to \mathrm{h}(\tau\tau)\mathrm{h_S}(\mathrm{bb})) = 200$ or 50 fb, depending on the $\tau\tau$ final state, is also shown by a red line.

In the middle panels for all background categories, the purity estimated for the background template of each corresponding event category is shown. For the signal categories, the ratio of the indicated signal divided by the sum of all backgrounds is shown. In the lower panels of each figure, the observed numbers of events divided by the numbers of events expected from the background model are shown for each bin.

JHEP11(2021)057

Uncertainty		Process				Correlated across	
		Sim.	τ-emb.	F_F	Variation	Years	Processes
τ-emb.	Acceptance	—	✓	—	4%	—	—
	$t\bar{t}$ fraction	—	✓	—	0.1–10%	—	—
μ	Id	✓	✓	—	2%	✓	✓
	Trigger	✓	✓	—	2.0%	—	✓
	p_μ scale	✓	✓	—	0.1–2.0%	✓	✓
e	Id	✓	✓	—	2%	✓	✓
	Trigger	✓	✓	—	2%	—	✓
	E_e scale	✓	✓	—	See text	✓	✓
τ_h	Id	✓	✓	—	3–5%	—	✓
	Trigger	✓	✓	—	5–10%	—	✓
	E_{τ_h} scale	✓	✓	—	0.2–1.1%	—	✓
$\mu \to \tau_h$	Miss-Id	✓	—	—	10–70%	—	—
	E_{τ_h} scale	✓	—	—	2%	—	—
$e \to \tau_h$	Miss-Id	✓	—	—	40%	—	—
	E_{τ_h} scale	✓	—	—	1.0–2.5%	—	—
Z boson p_T reweighting		✓	—	—	10–20%	✓	—
E_{Jet} scale & resolution		✓	—	—	0.1–10%	✓	✓
b-jet (miss-)Id		✓	—	—	1–10%	—	✓
p_T^{miss} calibration		✓	—	—	See text	✓	✓
ECAL timing shift		✓	—	—	2–3%	✓	✓
t quark p_T reweighting		✓	—	—	See text	✓	—
Luminosity		✓	—	—	2.3–2.5%	✓	✓
Process normalizations		✓	—	—	See text	✓	—
Signal acceptance		✓	—	—	18–20%	✓	—
F_F	Statistics	—	—	✓	3–5%	—	—
	Non-closure	—	—	✓	10%	—	—
	Non-F_F processes	—	—	✓	7%	—	—
	F_F proc. composition	—	—	✓	7%	—	—

Table 3. Summary of systematic uncertainties discussed in the text. The first column indicates the source of uncertainty; the second the processes that it applies to; the third the variation; and the last how it is correlated with other uncertainties. A checkmark is given also for partial correlations. More details are given in the text.

JHEP11(2021)057

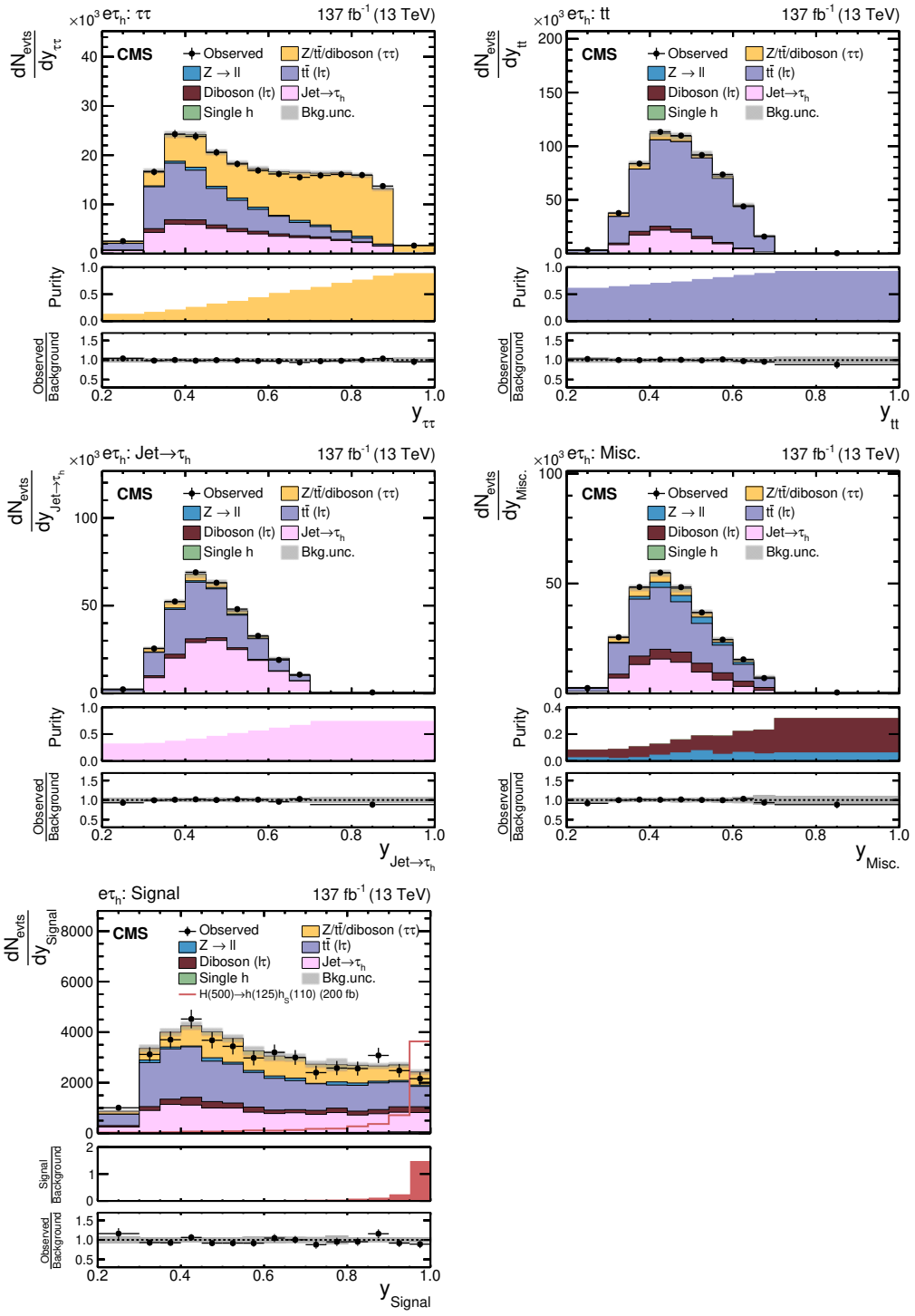

Figure 2. Event categories after NN classification based on a training for $m_{\mathrm{H}} = 500\,\mathrm{GeV}$ and $100 \leq m_{\mathrm{h_S}} < 150\,\mathrm{GeV}$ in the $\mathrm{e}\tau_{\mathrm{h}}$ final state. Shown are the (upper left) $\tau\tau$, (upper right) tt, (middle left) jet $\rightarrow \tau_{\mathrm{h}}$, (middle right) misc, and (lower left) signal categories. For these figures the data sets of all years have been combined. The uncertainty bands correspond to the combination of statistical and systematic uncertainties after the fit to the signal plus background hypothesis for $m_{\mathrm{H}} = 500\,\mathrm{GeV}$ and $m_{\mathrm{h_S}} = 110\,\mathrm{GeV}$.

JHEP11(2021)057

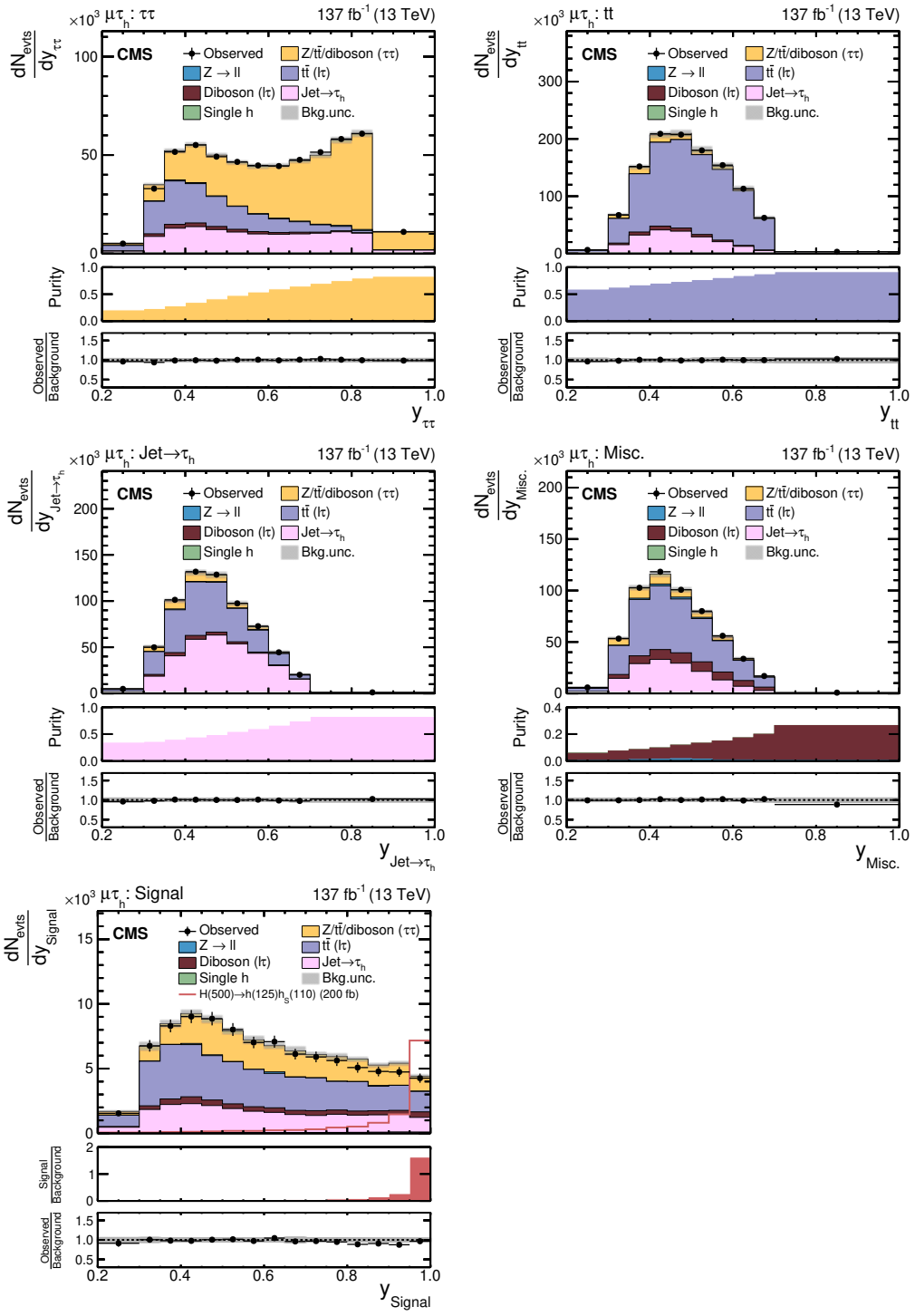

Figure 3. Event categories after NN classification based on a training for $m_{\mathrm{H}} = 500\,\mathrm{GeV}$ and $100 \leq m_{\mathrm{h_S}} < 150\,\mathrm{GeV}$ in the $\mu\tau_{\mathrm{h}}$ final state. Shown are the (upper left) $\tau\tau$, (upper right) tt, (middle left) jet $\to \tau_{\mathrm{h}}$, (middle right) misc, and (lower left) signal categories. For these figures the data sets of all years have been combined. The uncertainty bands correspond to the combination of statistical and systematic uncertainties after the fit to the signal plus background hypothesis for $m_{\mathrm{H}} = 500\,\mathrm{GeV}$ and $m_{\mathrm{h_S}} = 110\,\mathrm{GeV}$.

JHEP11(2021)057

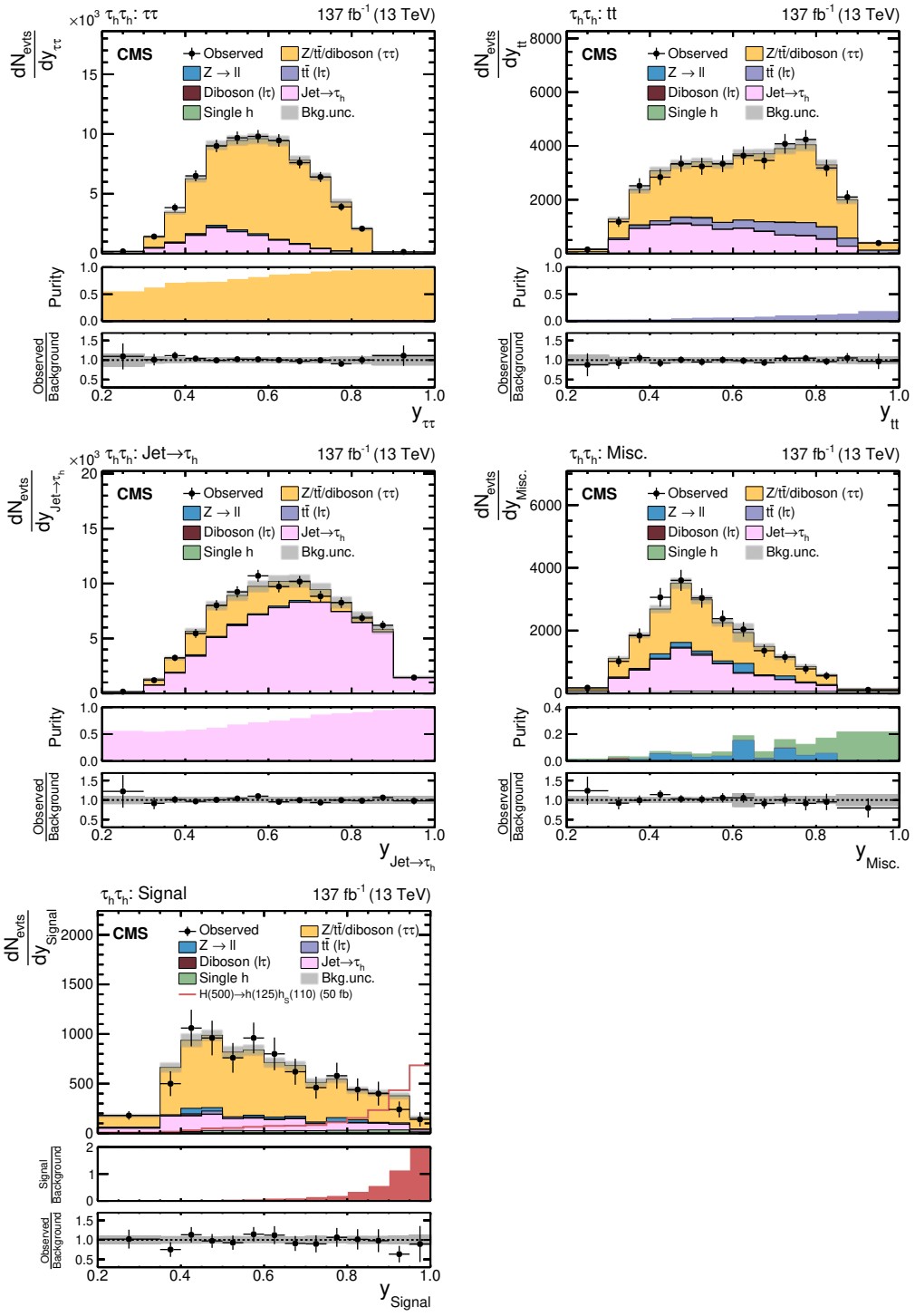

Figure 4. Event categories after NN classification based on a training for $m_{\mathrm{H}} = 500\,\mathrm{GeV}$ and $100 \leq m_{\mathrm{h_S}} < 150\,\mathrm{GeV}$ in the $\tau_{\mathrm{h}}\tau_{\mathrm{h}}$ final state. Shown are the (upper left) ττ, (upper right) tt, (middle left) jet $\rightarrow \tau_{\mathrm{h}}$, (middle right) misc, and (lower left) signal categories. For these figures the data sets of all years have been combined. The uncertainty bands correspond to the combination of statistical and systematic uncertainties after the fit to the signal plus background hypothesis for $m_{\mathrm{H}} = 500\,\mathrm{GeV}$ and $m_{\mathrm{h_S}} = 110\,\mathrm{GeV}$.

JHEP11(2021)057

No signal-like excess is observed in any of the investigated mass combinations and 95% confidence level (CL) upper limits on the $\sigma\,\mathcal{B}(\mathrm{H} \to \mathrm{h}(\tau\tau)\mathrm{h_S}(\mathrm{bb}))$ of a potential signal are set following the modified frequentist approach as described in refs. [89, 90], using the same definition of the profile likelihood test statistic as defined in refs. [88, 91]:

$$q_\mu = -2\ln\left(\frac{\mathcal{L}(\{k_i\}|\,\mu\,S_i(m_\mathrm{H},\,m_{\mathrm{h_S}},\,\{\hat{\theta}_{j,\mu}\}) + B_i(\{\hat{\theta}_{j,\mu}\}))}{\mathcal{L}(\{k_i\}|\,\hat{\mu}\,S_i(m_\mathrm{H},\,m_{\mathrm{h_S}},\,\{\hat{\theta}_{j,\hat{\mu}}\}) + B_i(\{\hat{\theta}_{j,\hat{\mu}}\}))}\right),\quad 0 \le \hat{\mu} \le \mu. \tag{7.2}$$

In eq. (7.2), $\hat{\mu}$, $\hat{\theta}_{j,\mu}$, and $\hat{\theta}_{j,\hat{\mu}}$ indicate the maximum likelihood estimates of the corresponding parameters from the fit to the data and the index of q_μ indicates that the fit to the data has been performed for a fixed value of μ. In the large number limit, the distribution of q_μ can be approximated by analytic functions, from which the median and the uncertainty contours can be obtained as described in ref. [92].

The observed and expected limits as a function of the tested values of $m_{\mathrm{h_S}}$ in a mass range from $240 \le m_\mathrm{H} \le 3000\,\mathrm{GeV}$ and for the combination of all $\tau\tau$ final states and the analyzed data from all years are shown in figure 5. The observed limits are given by the black points. The expected median values in the absence of signal are indicated by the dashed black line with the central 68 and 95% expected quantiles for the upper limit given by the green and yellow bands. They range from 125 fb for $m_\mathrm{H} = 240\,\mathrm{GeV}$ and $m_{\mathrm{h_S}} = 85\,\mathrm{GeV}$ to 2.7 fb for $m_\mathrm{H} = 1000\,\mathrm{GeV}$ and $m_{\mathrm{h_S}} = 350\,\mathrm{GeV}$ with a roughly flattening progression beyond. These limits are model independent. Since the analysis is not able to distinguish between scalar and pseudoscalar Higgs bosons, the limits are equally applicable to both cases. Residual differences on the detector acceptance for a scalar or pseudoscalar $\mathrm{h_S}$ are expected to be small and well covered by the theoretical acceptance uncertainties discussed in section 6.

It should be noted that neighboring points in $m_{\mathrm{h_S}}$ differ only slightly in the kinematic properties of the tested signal hypotheses. Groups of hypothesis tests based on the same NN trainings for classification are indicated by discontinuities in the limits, which are linearly connected otherwise to improve the visibility of common trends.

A summary of the observed limits for all tested pairs of m_H and $m_{\mathrm{h_S}}$ is shown in figure 6, where the limits are given by the color code of the figure.

Maximally allowed values for $\sigma\,\mathcal{B}(\mathrm{H} \to \mathrm{h}(\tau\tau)\mathrm{h_S}(\mathrm{bb}))$ in the context of the NMSSM for given pairs m_H and $m_{\mathrm{h_S}}$, have been provided by the LHC Higgs Working Group, using the codes NMSSMTools 5.5.0 [93] and NMSSMCALC [94], incorporating experimental constraints from measurements of the h properties, SUSY searches, B-meson physics and dark matter searches. The region in the plane spanned by m_H and $m_{\mathrm{h_S}}$ where the observed limits fall below these maximally allowed values on $\sigma\,\mathcal{B}(\mathrm{H} \to \mathrm{h}(\tau\tau)\mathrm{h_S}(\mathrm{bb}))$ are indicated by a read hatched area. It corresponds to $400 \le m_\mathrm{H} \lesssim 600\,\mathrm{GeV}$ and $60 \le m_{\mathrm{h_S}} \lesssim 200\,\mathrm{GeV}$. For $m(\mathrm{H}) = 450\,\mathrm{GeV}$ and $60 \le m_{\mathrm{h_S}} \le 80\,\mathrm{GeV}$ the observed limits are five times smaller than the maximally allowed values for $\sigma\,\mathcal{B}(\mathrm{H} \to \mathrm{h}(\tau\tau)\mathrm{h_S}(\mathrm{bb}))$. Tabulated results of this analysis are available in the HepData database [95].

JHEP11(2021)057

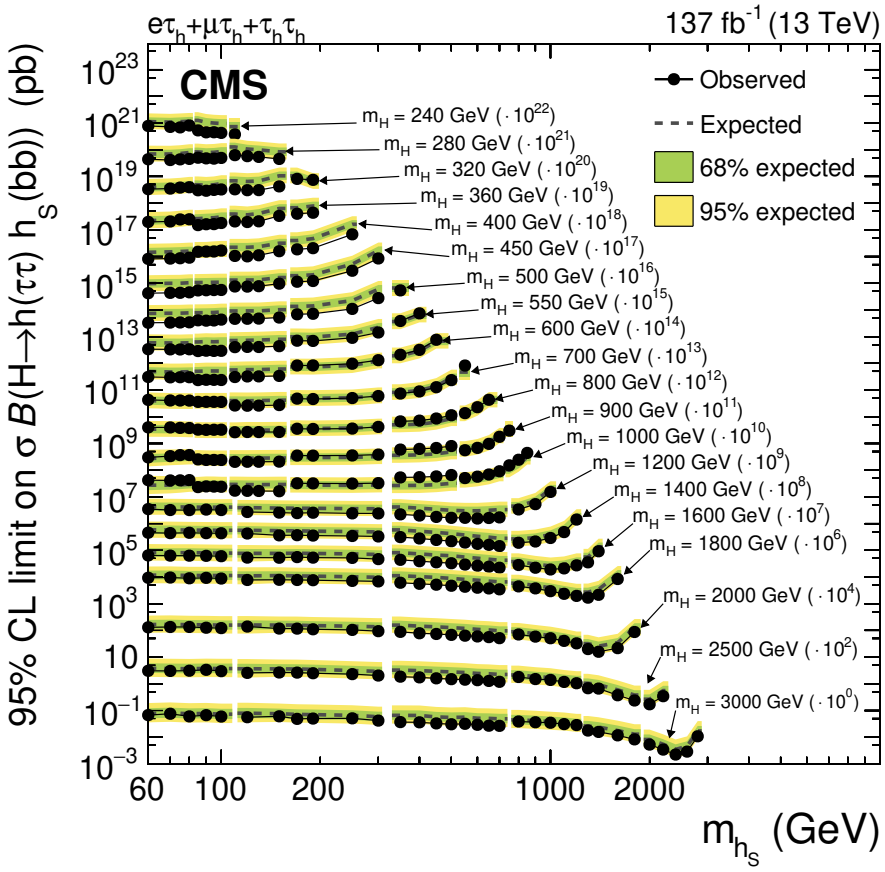

Figure 5. Expected and observed 95% CL upper limits on $\sigma\mathcal{B}(\mathrm{H} \to \mathrm{h}(\tau\tau)\mathrm{h_S}(\mathrm{bb}))$ for all tested values of m_H and $m_{\mathrm{h_S}}$. The limits for each corresponding mass value have been scaled by orders of ten as indicated in the annotations. Groups of hypothesis tests based on the same NN trainings for classification are indicated by discontinuities in the limits, which are linearly connected otherwise to improve the visibility of common trends.

8 Summary

A search for a heavy Higgs boson H decaying into the observed Higgs boson h with a mass of 125 GeV and another Higgs boson $\mathrm{h_S}$ has been presented. The h and $\mathrm{h_S}$ bosons are required to decay into a pair of tau leptons and a pair of b quarks, respectively. The search uses a sample of proton-proton collisions collected with the CMS detector at a center-of-mass energy of 13 TeV, corresponding to an integrated luminosity of 137 fb^{-1}. Mass ranges of 240–3000 GeV for m_H and 60–2800 GeV for $m_{\mathrm{h_S}}$ are explored in the search. No signal has been observed. Model independent 95% confidence level upper limits on the product of the production cross section and the branching fractions of the signal process are set with a sensitivity ranging from 125 fb (for $m_\mathrm{H} = 240$ GeV) to 2.7 fb (for $m_\mathrm{H} = 1000$ GeV). These limits have been compared to maximally allowed products of the production cross section and the branching fractions of the signal process in the next-to-minimal supersymmetric extension of the standard model. This is the first search for such a process carried out at the LHC.

JHEP11(2021)057

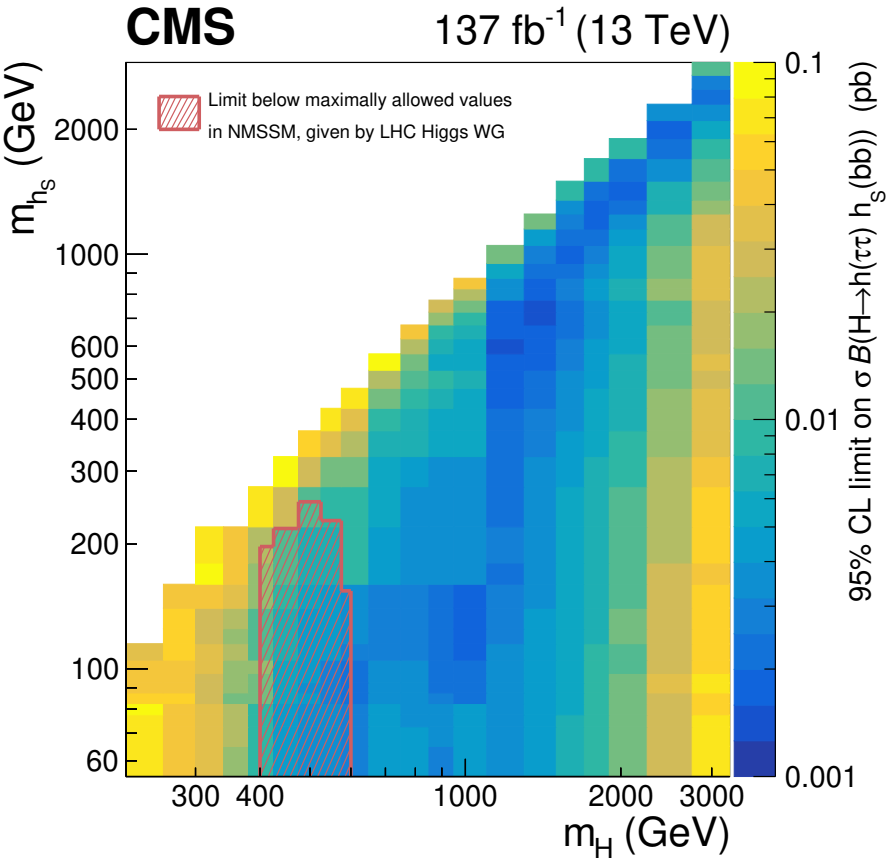

Figure 6. Summary of the observed limits on $\sigma\,\mathcal{B}(\mathrm{H} \to \mathrm{h}(\tau\tau)\mathrm{h_S}(\mathrm{bb}))$ for all tested pairs of m_{H} and $m_{\mathrm{h_S}}$, as shown in figure 5. The limits are given by the color code of the figure. The region in the plane spanned by m_{H} and $m_{\mathrm{h_S}}$ where the observed limits fall below the maximally allowed values on $\sigma\,\mathcal{B}(\mathrm{H} \to \mathrm{h}(\tau\tau)\mathrm{h_S}(\mathrm{bb}))$ in the context of the NMSSM, as provided by the LHC Higgs Working Group, are indicated by a red hatched area.

Acknowledgments

We congratulate our colleagues in the CERN accelerator departments for the excellent performance of the LHC and thank the technical and administrative staffs at CERN and at other CMS institutes for their contributions to the success of the CMS effort. In addition, we gratefully acknowledge the computing centers and personnel of the Worldwide LHC Computing Grid and other centers for delivering so effectively the computing infrastructure essential to our analyses. Finally, we acknowledge the enduring support for the construction and operation of the LHC, the CMS detector, and the supporting computing infrastructure provided by the following funding agencies: BMBWF and FWF (Austria); FNRS and FWO (Belgium); CNPq, CAPES, FAPERJ, FAPERGS, and FAPESP (Brazil); MES (Bulgaria); CERN; CAS, MoST, and NSFC (China); MINCIENCIAS (Colombia); MSES and CSF (Croatia); RIF (Cyprus); SENESCYT (Ecuador); MoER, ERC PUT and ERDF (Estonia); Academy of Finland, MEC, and HIP (Finland); CEA and CNRS/IN2P3

JHEP11(2021)057

(France); BMBF, DFG, and HGF (Germany); GSRT (Greece); NKFIA (Hungary); DAE and DST (India); IPM (Iran); SFI (Ireland); INFN (Italy); MSIP and NRF (Republic of Korea); MES (Latvia); LAS (Lithuania); MOE and UM (Malaysia); BUAP, CINVESTAV, CONACYT, LNS, SEP, and UASLP-FAI (Mexico); MOS (Montenegro); MBIE (New Zealand); PAEC (Pakistan); MSHE and NSC (Poland); FCT (Portugal); JINR (Dubna); MON, RosAtom, RAS, RFBR, and NRC KI (Russia); MESTD (Serbia); SEIDI, CPAN, PCTI, and FEDER (Spain); MOSTR (Sri Lanka); Swiss Funding Agencies (Switzerland); MST (Taipei); ThEPCenter, IPST, STAR, and NSTDA (Thailand); TUBITAK and TAEK (Turkey); NASU (Ukraine); STFC (United Kingdom); DOE and NSF (U.S.A.).

Individuals have received support from the Marie-Curie program and the European Research Council and Horizon 2020 Grant, contract Nos. 675440, 724704, 752730, 765710 and 824093 (European Union); the Leventis Foundation; the Alfred P. Sloan Foundation; the Alexander von Humboldt Foundation; the Belgian Federal Science Policy Office; the Fonds pour la Formation à la Recherche dans l'Industrie et dans l'Agriculture (FRIA-Belgium); the Agentschap voor Innovatie door Wetenschap en Technologie (IWT-Belgium); the F.R.S.-FNRS and FWO (Belgium) under the "Excellence of Science — EOS" — be.h project n. 30820817; the Beijing Municipal Science & Technology Commission, No. Z191100007219010; the Ministry of Education, Youth and Sports (MEYS) of the Czech Republic; the Deutsche Forschungsgemeinschaft (DFG), under Germany's Excellence Strategy — EXC 2121 "Quantum Universe" — 390833306, and under project number 400140256 — GRK2497; the Lendület ("Momentum") Program and the János Bolyai Research Scholarship of the Hungarian Academy of Sciences, the New National Excellence Program ÚNKP, the NKFIA research grants 123842, 123959, 124845, 124850, 125105, 128713, 128786, and 129058 (Hungary); the Council of Science and Industrial Research, India; the Latvian Council of Science; the Ministry of Science and Higher Education and the National Science Center, contracts Opus 2014/15/B/ST2/03998 and 2015/19/B/ST2/02861 (Poland); the National Priorities Research Program by Qatar National Research Fund; the Ministry of Science and Higher Education, project no. 0723-2020-0041 (Russia); the Programa Estatal de Fomento de la Investigación Científica y Técnica de Excelencia María de Maeztu, grant MDM-2015-0509 and the Programa Severo Ochoa del Principado de Asturias; the Thalis and Aristeia programs cofinanced by EU-ESF and the Greek NSRF; the Rachadapisek Sompot Fund for Postdoctoral Fellowship, Chulalongkorn University and the Chulalongkorn Academic into Its 2nd Century Project Advancement Project (Thailand); the Kavli Foundation; the Nvidia Corporation; the SuperMicro Corporation; the Welch Foundation, contract C-1845; and the Weston Havens Foundation (U.S.A.).

JHEP11(2021)057

References

[1] ATLAS collaboration, *Observation of a new particle in the search for the Standard Model Higgs boson with the ATLAS detector at the LHC*, *Phys. Lett. B* **716** (2012) 1 [arXiv:1207.7214] [INSPIRE].

[2] CMS collaboration, *Observation of a new boson at a mass of* 125 *GeV with the CMS experiment at the LHC*, *Phys. Lett. B* **716** (2012) 30 [arXiv:1207.7235] [INSPIRE].

[3] CMS collaboration, *Observation of a new boson with mass near* 125 *GeV in pp collisions at* $\sqrt{s} = 7$ *and* 8 *TeV*, *JHEP* **06** (2013) 081 [arXiv:1303.4571] [INSPIRE].

[4] ATLAS, CMS collaboration, *Measurements of the Higgs boson production and decay rates and constraints on its couplings from a combined ATLAS and CMS analysis of the LHC pp collision data at* $\sqrt{s} = 7$ *and* 8 *TeV*, *JHEP* **08** (2016) 045 [arXiv:1606.02266] [INSPIRE].

[5] CMS collaboration, *Combined measurements of Higgs boson couplings in proton-proton collisions at* $\sqrt{s} = 13$ *TeV*, *Eur. Phys. J. C* **79** (2019) 421 [arXiv:1809.10733] [INSPIRE].

[6] ATLAS collaboration, *Combined measurements of Higgs boson production and decay using up to* $80\,fb^{-1}$ *of proton-proton collision data at* $\sqrt{s} = 13$ *TeV collected with the ATLAS experiment*, *Phys. Rev. D* **101** (2020) 012002 [arXiv:1909.02845] [INSPIRE].

[7] CMS collaboration, *Measurements of the Higgs boson width and anomalous HVV couplings from on-shell and off-shell production in the four-lepton final state*, *Phys. Rev. D* **99** (2019) 112003 [arXiv:1901.00174] [INSPIRE].

[8] Y.A. Golfand and E.P. Likhtman, *Extension of the algebra of Poincaré group generators and violation of p invariance*, *JETP Lett.* **13** (1971) 323 [*Pisma Zh. Eksp. Teor. Fiz.* **13** (1971) 452] [INSPIRE].

[9] J. Wess and B. Zumino, *Supergauge transformations in four-dimensions*, *Nucl. Phys. B* **70** (1974) 39 [INSPIRE].

[10] P.W. Higgs, *Broken symmetries, massless particles and gauge fields*, *Phys. Lett.* **12** (1964) 132 [INSPIRE].

[11] P.W. Higgs, *Broken symmetries and the masses of gauge bosons*, *Phys. Rev. Lett.* **13** (1964) 508 [INSPIRE].

[12] G.S. Guralnik, C.R. Hagen and T.W.B. Kibble, *Global conservation laws and massless particles*, *Phys. Rev. Lett.* **13** (1964) 585 [INSPIRE].

[13] F. Englert and R. Brout, *Broken symmetry and the mass of gauge vector mesons*, *Phys. Rev. Lett.* **13** (1964) 321 [INSPIRE].

[14] P.W. Higgs, *Spontaneous symmetry breakdown without massless bosons*, *Phys. Rev.* **145** (1966) 1156 [INSPIRE].

[15] T.W.B. Kibble, *Symmetry breaking in non-Abelian gauge theories*, *Phys. Rev.* **155** (1967) 1554 [INSPIRE].

[16] P. Fayet, *Supergauge invariant extension of the Higgs mechanism and a model for the electron and its neutrino*, *Nucl. Phys. B* **90** (1975) 104 [INSPIRE].

[17] P. Fayet, *Spontaneously broken supersymmetric theories of weak, electromagnetic and strong interactions*, *Phys. Lett. B* **69** (1977) 489 [INSPIRE].

JHEP11(2021)057

[18] J.E. Kim and H.P. Nilles, *The μ problem and the strong CP problem*, *Phys. Lett. B* **138** (1984) 150 [INSPIRE].

[19] U. Ellwanger, C. Hugonie and A.M. Teixeira, *The next-to-minimal supersymmetric standard model*, *Phys. Rept.* **496** (2010) 1 [arXiv:0910.1785] [INSPIRE].

[20] M. Maniatis, *The next-to-minimal supersymmetric extension of the standard model reviewed*, *Int. J. Mod. Phys. A* **25** (2010) 3505 [arXiv:0906.0777] [INSPIRE].

[21] ATLAS collaboration, *Search for heavy Higgs bosons decaying into two tau leptons with the ATLAS detector using pp collisions at $\sqrt{s} = 13$ TeV*, *Phys. Rev. Lett.* **125** (2020) 051801 [arXiv:2002.12223] [INSPIRE].

[22] CMS collaboration, *Search for additional neutral MSSM Higgs bosons in the $\tau\tau$ final state in proton-proton collisions at $\sqrt{s} = 13$ TeV*, *JHEP* **09** (2018) 007 [arXiv:1803.06553] [INSPIRE].

[23] ATLAS collaboration, *Search for charged Higgs bosons decaying via $H^{\pm} \to \tau^{\pm}\nu_{\tau}$ in the τ+jets and τ+lepton final states with 36 fb^{-1} of pp collision data recorded at $\sqrt{s} = 13$ TeV with the ATLAS experiment*, *JHEP* **09** (2018) 139 [arXiv:1807.07915] [INSPIRE].

[24] CMS collaboration, *Search for charged Higgs bosons in the $H^{\pm} \to \tau^{\pm}\nu_{\tau}$ decay channel in proton-proton collisions at $\sqrt{s} = 13$ TeV*, *JHEP* **07** (2019) 142 [arXiv:1903.04560] [INSPIRE].

[25] S.F. King, M. Mühlleitner, R. Nevzorov and K. Walz, *Discovery prospects for NMSSM Higgs bosons at the high-energy Large Hadron Collider*, *Phys. Rev. D* **90** (2014) 095014 [arXiv:1408.1120] [INSPIRE].

[26] CMS collaboration, *Description and performance of track and primary-vertex reconstruction with the CMS tracker*, 2014 *JINST* **9** P10009 [arXiv:1405.6569] [INSPIRE].

[27] CMS collaboration, *Track impact parameter resolution for the full pseudo rapidity coverage in the* 2017 *dataset with the CMS phase-*1 *pixel detector*, CMS-DP-2020-049, CERN, Geneva, Switzerland (2020).

[28] CMS collaboration, *Performance of electron reconstruction and selection with the CMS detector in proton-proton collisions at $\sqrt{s} = 8$ TeV*, 2015 *JINST* **10** P06005 [arXiv:1502.02701] [INSPIRE].

[29] CMS collaboration, *Performance of CMS muon reconstruction in pp collision events at $\sqrt{s} = 7$ TeV*, 2012 *JINST* **7** P10002 [arXiv:1206.4071] [INSPIRE].

[30] CMS collaboration, *Performance of photon reconstruction and identification with the CMS detector in proton-proton collisions at $\sqrt{s} = 8$ TeV*, 2015 *JINST* **10** P08010 [arXiv:1502.02702] [INSPIRE].

[31] CMS collaboration, *Jet energy scale and resolution in the CMS experiment in pp collisions at* 8 *TeV*, 2017 *JINST* **12** P02014 [arXiv:1607.03663] [INSPIRE].

[32] CMS collaboration, *Performance of the CMS level-*1 *trigger in proton-proton collisions at $\sqrt{s} = 13$ TeV*, 2020 *JINST* **15** P10017 [arXiv:2006.10165] [INSPIRE].

[33] CMS collaboration, *The CMS trigger system*, 2017 *JINST* **12** P01020 [arXiv:1609.02366] [INSPIRE].

[34] CMS collaboration, *The CMS experiment at the CERN LHC*, 2008 *JINST* **3** S08004 [INSPIRE].

JHEP11(2021)057

[35] CMS collaboration, *Particle-flow reconstruction and global event description with the CMS detector*, 2017 *JINST* **12** P10003 [arXiv:1706.04965] [INSPIRE].

[36] M. Cacciari, G.P. Salam and G. Soyez, *FastJet user manual*, *Eur. Phys. J. C* **72** (2012) 1896 [arXiv:1111.6097] [INSPIRE].

[37] CMS collaboration, *Electron and photon reconstruction and identification with the CMS experiment at the CERN LHC*, 2021 *JINST* **16** P05014 [arXiv:2012.06888] [INSPIRE].

[38] CMS collaboration, *Performance of the CMS muon detector and muon reconstruction with proton-proton collisions at* $\sqrt{s} = 13$ *TeV*, 2018 *JINST* **13** P06015 [arXiv:1804.04528] [INSPIRE].

[39] CMS collaboration, *Identification of heavy-flavour jets with the CMS detector in pp collisions at* 13 *TeV*, 2018 *JINST* **13** P05011 [arXiv:1712.07158] [INSPIRE].

[40] E. Bols, J. Kieseler, M. Verzetti, M. Stoye and A. Stakia, *Jet flavour classification using DeepJet*, 2020 *JINST* **15** P12012 [arXiv:2008.10519] [INSPIRE].

[41] CMS collaboration, *Performance of the DeepJet b tagging algorithm using* $41.9\,fb^{-1}$ *of data from proton-proton collisions at* 13 *TeV with phase* 1 *CMS detector*, CMS-DP-2018-058, CERN, Geneva, Switzerland (2018).

[42] CMS collaboration, *Performance of reconstruction and identification of* τ *leptons decaying to hadrons and* ν_τ *in pp collisions at* $\sqrt{s} = 13$ *TeV*, 2018 *JINST* **13** P10005 [arXiv:1809.02816] [INSPIRE].

[43] CMS collaboration, *Performance of the DeepTau algorithm for the discrimination of taus against jets, electron, and muons*, CMS-DP-2019-033, CERN, Geneva, Switzerland (2019).

[44] D. Bertolini, P. Harris, M. Low and N. Tran, *Pileup per particle identification*, *JHEP* **10** (2014) 059 [arXiv:1407.6013] [INSPIRE].

[45] CMS collaboration, *Performance of missing transverse momentum reconstruction in proton-proton collisions at* $\sqrt{s} = 13$ *TeV using the CMS detector*, 2019 *JINST* **14** P07004 [arXiv:1903.06078] [INSPIRE].

[46] CMS collaboration, *An embedding technique to determine* $\tau\tau$ *backgrounds in proton-proton collision data*, 2019 *JINST* **14** P06032 [arXiv:1903.01216] [INSPIRE].

[47] CMS collaboration, *Measurement of the* $Z\gamma^* \to \tau\tau$ *cross section in pp collisions at* $\sqrt{s} = 13$ *TeV and validation of* τ *lepton analysis techniques*, *Eur. Phys. J. C* **78** (2018) 708 [arXiv:1801.03535] [INSPIRE].

[48] J. Alwall, M. Herquet, F. Maltoni, O. Mattelaer and T. Stelzer, *MadGraph* 5*: going beyond*, *JHEP* **06** (2011) 128 [arXiv:1106.0522] [INSPIRE].

[49] J. Alwall et al., *The automated computation of tree-level and next-to-leading order differential cross sections, and their matching to parton shower simulations*, *JHEP* **07** (2014) 079 [arXiv:1405.0301] [INSPIRE].

[50] P. Nason, *A new method for combining NLO QCD with shower Monte Carlo algorithms*, *JHEP* **11** (2004) 040 [hep-ph/0409146] [INSPIRE].

[51] S. Frixione, P. Nason and C. Oleari, *Matching NLO QCD computations with parton shower simulations: the POWHEG method*, *JHEP* **11** (2007) 070 [arXiv:0709.2092] [INSPIRE].

[52] S. Alioli, P. Nason, C. Oleari and E. Re, *NLO Higgs boson production via gluon fusion matched with shower in POWHEG*, *JHEP* **04** (2009) 002 [arXiv:0812.0578] [INSPIRE].

JHEP11(2021)057

[53] S. Alioli, P. Nason, C. Oleari and E. Re, *A general framework for implementing NLO calculations in shower Monte Carlo programs: the POWHEG BOX*, *JHEP* **06** (2010) 043 [arXiv:1002.2581] [INSPIRE].

[54] S. Alioli, K. Hamilton, P. Nason, C. Oleari and E. Re, *Jet pair production in POWHEG*, *JHEP* **04** (2011) 081 [arXiv:1012.3380] [INSPIRE].

[55] E. Bagnaschi, G. Degrassi, P. Slavich and A. Vicini, *Higgs production via gluon fusion in the POWHEG approach in the SM and in the MSSM*, *JHEP* **02** (2012) 088 [arXiv:1111.2854] [INSPIRE].

[56] K. Melnikov and F. Petriello, *Electroweak gauge boson production at hadron colliders through* $O(\alpha_s^2)$, *Phys. Rev. D* **74** (2006) 114017 [hep-ph/0609070] [INSPIRE].

[57] M. Czakon and A. Mitov, *Top++: a program for the calculation of the top-pair cross-section at hadron colliders*, *Comput. Phys. Commun.* **185** (2014) 2930 [arXiv:1112.5675] [INSPIRE].

[58] N. Kidonakis, *Top quark production*, in *Helmholtz international summer school on physics of heavy quarks and hadrons*, DESY-PROC-2013-03, (2014), pg. 139 [arXiv:1311.0283] [INSPIRE].

[59] J.M. Campbell, R.K. Ellis and C. Williams, *Vector boson pair production at the LHC*, *JHEP* **07** (2011) 018 [arXiv:1105.0020] [INSPIRE].

[60] T. Gehrmann et al., W^+W^- *production at hadron colliders in next to next to leading order QCD*, *Phys. Rev. Lett.* **113** (2014) 212001 [arXiv:1408.5243] [INSPIRE].

[61] NNPDF collaboration, *Parton distributions for the LHC run II*, *JHEP* **04** (2015) 040 [arXiv:1410.8849] [INSPIRE].

[62] NNPDF collaboration, *Parton distributions from high-precision collider data*, *Eur. Phys. J. C* **77** (2017) 663 [arXiv:1706.00428] [INSPIRE].

[63] CMS collaboration, *Event generator tunes obtained from underlying event and multiparton scattering measurements*, *Eur. Phys. J. C* **76** (2016) 155 [arXiv:1512.00815] [INSPIRE].

[64] CMS collaboration, *Extraction and validation of a new set of CMS PYTHIA 8 tunes from underlying-event measurements*, *Eur. Phys. J. C* **80** (2020) 4 [arXiv:1903.12179] [INSPIRE].

[65] T. Sjöstrand et al., *An introduction to PYTHIA 8.2*, *Comput. Phys. Commun.* **191** (2015) 159 [arXiv:1410.3012] [INSPIRE].

[66] GEANT4 collaboration, *GEANT4 — a simulation toolkit*, *Nucl. Instrum. Meth. A* **506** (2003) 250 [INSPIRE].

[67] CMS collaboration, *Measurements of inclusive W and Z cross sections in pp collisions at* $\sqrt{s} = 7$ *TeV*, *JHEP* **01** (2011) 080 [arXiv:1012.2466] [INSPIRE].

[68] CMS collaboration, *Measurement of the differential cross section for top quark pair production in pp collisions at* $\sqrt{s} = 8$ *TeV*, *Eur. Phys. J. C* **75** (2015) 542 [arXiv:1505.04480] [INSPIRE].

[69] S. Baker and R.D. Cousins, *Clarification of the use of* χ *square and likelihood functions in fits to histograms*, *Nucl. Instrum. Meth.* **221** (1984) 437 [INSPIRE].

[70] CMS collaboration, *A deep neural network for simultaneous estimation of b jet energy and resolution*, *Comput. Softw. Big Sci.* **4** (2020) 10 [arXiv:1912.06046] [INSPIRE].

[71] M. Abadi et al., *TensorFlow: large-scale machine learning on heterogeneous systems*, https://www.tensorflow.org/, (2015).

JHEP11(2021)057

[72] L. Bianchini, J. Conway, E.K. Friis and C. Veelken, *Reconstruction of the Higgs mass in $H \to \tau\tau$ events by dynamical likelihood techniques*, *J. Phys. Conf. Ser.* **513** (2014) 022035 [INSPIRE].

[73] CMS collaboration, *Searches for a heavy scalar boson H decaying to a pair of 125 GeV Higgs bosons hh or for a heavy pseudoscalar boson A decaying to Zh, in the final states with $h \to \tau\tau$*, *Phys. Lett. B* **755** (2016) 217 [arXiv:1510.01181] [INSPIRE].

[74] S. Wunsch, R. Friese, R. Wolf and G. Quast, *Identifying the relevant dependencies of the neural network response on characteristics of the input space*, *Comput. Softw. Big Sci.* **2** (2018) 5 [arXiv:1803.08782] [INSPIRE].

[75] X. Glorot and Y. Bengio, *Understanding the difficulty of training deep feedforward neural networks*, in *Proceedings of the thirteenth international conference on artificial intelligence and statistics*, Y.W. Teh and M. Titterington eds., *Proceedings of machine learning research* **9**, Chia Laguna Resort, Sardinia, Italy, 13–15 May 2010, pg. 249.

[76] R. Shimizu et al., *Balanced mini-batch training for imbalanced image data classification with neural network*, in 2018 *First International Conference on Artificial Intelligence for Industries*, (AI4I), (2018), pg. 27.

[77] D.P. Kingma and J. Ba, *Adam: a method for stochastic optimization*, arXiv:1412.6980 [INSPIRE].

[78] A.N. Tikhonov, *Solution of incorrectly formulated problems and the regularization method*, *Soviet Math. Dokl.* **4** (1963) 1035.

[79] R.J. Barlow and C. Beeston, *Fitting using finite Monte Carlo samples*, *Comput. Phys. Commun.* **77** (1993) 219 [INSPIRE].

[80] CMS collaboration, *Precision luminosity measurement in proton-proton collisions at $\sqrt{s} = 13$ TeV in* 2015 *and* 2016 *at CMS*, *Eur. Phys. J. C* **81** (2021) 800 [arXiv:2104.01927] [INSPIRE].

[81] CMS collaboration, *CMS luminosity measurement for the* 2017 *data-taking period at $\sqrt{s} = 13$ TeV*, Tech. Rep. CMS-PAS-LUM-17-004, CERN, Geneva, Switzerland (2018).

[82] CMS collaboration, *CMS luminosity measurements for the* 2016 *data taking period*, Tech. Rep. CMS-PAS-LUM-17-001, CERN, Geneva, Switzerland (2017).

[83] CMS collaboration, *CMS luminosity measurement for the* 2018 *data-taking period at $\sqrt{s} = 13$ TeV*, Tech. Rep. CMS-PAS-LUM-18-002, CERN, Geneva, Switzerland (2019).

[84] P. Nason and C. Oleari, *NLO Higgs boson production via vector-boson fusion matched with shower in POWHEG*, *JHEP* **02** (2010) 037 [arXiv:0911.5299] [INSPIRE].

[85] G. Luisoni, P. Nason, C. Oleari and F. Tramontano, *$HW^{\pm}/HZ + 0$ and 1 jet at NLO with the POWHEG BOX interfaced to GoSam and their merging within MiNLO*, *JHEP* **10** (2013) 083 [arXiv:1306.2542] [INSPIRE].

[86] H.B. Hartanto, B. Jager, L. Reina and D. Wackeroth, *Higgs boson production in association with top quarks in the POWHEG BOX*, *Phys. Rev. D* **91** (2015) 094003 [arXiv:1501.04498] [INSPIRE].

[87] LHC Higgs Cross Section Working Group collaboration, *Handbook of LHC Higgs cross sections: 4. Deciphering the nature of the Higgs sector*, Tech. Rep. CERN-2017-002-M, CERN, Geneva, Switzerland (2016) [CERN-2017-002].

JHEP11(2021)057

[88] ATLAS, CMS and LHC Higgs Combination Group collaborations, *Procedure for the LHC Higgs boson search combination in Summer* 2011, Tech. Rep. CMS-NOTE-2011-005, CERN, Geneva, Switzerland (2011) [ATL-PHYS-PUB-2011-11].

[89] T. Junk, *Confidence level computation for combining searches with small statistics*, *Nucl. Instrum. Meth. A* **434** (1999) 435 [hep-ex/9902006] [INSPIRE].

[90] A.L. Read, *Presentation of search results: the CL_s technique*, *J. Phys. G* **28** (2002) 2693 [INSPIRE].

[91] CMS collaboration, *Combined results of searches for the standard model Higgs boson in pp collisions at $\sqrt{s} = 7$ TeV*, *Phys. Lett. B* **710** (2012) 26 [arXiv:1202.1488] [INSPIRE].

[92] G. Cowan, K. Cranmer, E. Gross and O. Vitells, *Asymptotic formulae for likelihood-based tests of new physics*, *Eur. Phys. J. C* **71** (2011) 1554 [*Erratum ibid.* **73** (2013) 2501] [arXiv:1007.1727] [INSPIRE].

[93] U. Ellwanger and C. Hugonie, *NMHDECAY* 2.0*: an updated program for sparticle masses, Higgs masses, couplings and decay widths in the NMSSM*, *Comput. Phys. Commun.* **175** (2006) 290 [hep-ph/0508022] [INSPIRE].

[94] J. Baglio et al., *NMSSMCALC: a program package for the calculation of loop-corrected Higgs boson masses and decay widths in the (complex) NMSSM*, *Comput. Phys. Commun.* **185** (2014) 3372 [arXiv:1312.4788] [INSPIRE].

[95] *HEPData record for this analysis*, CMS-HIG-20-014, (2021).

JHEP11(2021)057

The CMS collaboration

Yerevan Physics Institute, Yerevan, Armenia

A. Tumasyan

Institut für Hochenergiephysik, Wien, Austria

W. Adam, J.W. Andrejkovic, T. Bergauer, S. Chatterjee, M. Dragicevic, A. Escalante Del Valle, R. Frühwirth[1], M. Jeitler[1], N. Krammer, L. Lechner, D. Liko, I. Mikulec, P. Paulitsch, F.M. Pitters, J. Schieck[1], R. Schöfbeck, M. Spanring, S. Templ, W. Waltenberger, C.-E. Wulz[1]

Institute for Nuclear Problems, Minsk, Belarus

V. Chekhovsky, A. Litomin, V. Makarenko

Universiteit Antwerpen, Antwerpen, Belgium

M.R. Darwish[2], E.A. De Wolf, T. Janssen, T. Kello[3], A. Lelek, H. Rejeb Sfar, P. Van Mechelen, S. Van Putte, N. Van Remortel

Vrije Universiteit Brussel, Brussel, Belgium

F. Blekman, E.S. Bols, J. D'Hondt, J. De Clercq, M. Delcourt, H. El Faham, S. Lowette, S. Moortgat, A. Morton, D. Müller, A.R. Sahasransu, S. Tavernier, W. Van Doninck, P. Van Mulders

Université Libre de Bruxelles, Bruxelles, Belgium

D. Beghin, B. Bilin, B. Clerbaux, G. De Lentdecker, L. Favart, A. Grebenyuk, A.K. Kalsi, K. Lee, M. Mahdavikhorrami, I. Makarenko, L. Moureaux, L. Pétré, A. Popov, N. Postiau, E. Starling, L. Thomas, M. Vanden Bemden, C. Vander Velde, P. Vanlaer, D. Vannerom, L. Wezenbeek

Ghent University, Ghent, Belgium

T. Cornelis, D. Dobur, J. Knolle, L. Lambrecht, G. Mestdach, M. Niedziela, C. Roskas, A. Samalan, K. Skovpen, M. Tytgat, W. Verbeke, B. Vermassen, M. Vit

Université Catholique de Louvain, Louvain-la-Neuve, Belgium

A. Bethani, G. Bruno, F. Bury, C. Caputo, P. David, C. Delaere, I.S. Donertas, A. Giammanco, K. Jaffel, Sa. Jain, V. Lemaitre, K. Mondal, J. Prisciandaro, A. Taliercio, M. Teklishyn, T.T. Tran, P. Vischia, S. Wertz

Centro Brasileiro de Pesquisas Fisicas, Rio de Janeiro, Brazil

G.A. Alves, C. Hensel, A. Moraes

Universidade do Estado do Rio de Janeiro, Rio de Janeiro, Brazil

W.L. Aldá Júnior, M. Alves Gallo Pereira, M. Barroso Ferreira Filho, H. Brandao Malbouisson, W. Carvalho, J. Chinellato[4], E.M. Da Costa, G.G. Da Silveira[5], D. De Jesus Damiao, S. Fonseca De Souza, D. Matos Figueiredo, C. Mora Herrera, K. Mota Amarilo, L. Mundim, H. Nogima, P. Rebello Teles, A. Santoro, S.M. Silva Do Amaral, A. Sznajder, M. Thiel, F. Torres Da Silva De Araujo, A. Vilela Pereira

JHEP11(2021)057

Universidade Estadual Paulista [a], Universidade Federal do ABC [b], São Paulo, Brazil

C.A. Bernardes[a,a,5], L. Calligaris[a], T.R. Fernandez Perez Tomei[a], E.M. Gregores[a,b], D.S. Lemos[a], P.G. Mercadante[a,b], S.F. Novaes[a], Sandra S. Padula[a]

Institute for Nuclear Research and Nuclear Energy, Bulgarian Academy of Sciences, Sofia, Bulgaria

A. Aleksandrov, G. Antchev, R. Hadjiiska, P. Iaydjiev, M. Misheva, M. Rodozov, M. Shopova, G. Sultanov

University of Sofia, Sofia, Bulgaria

A. Dimitrov, T. Ivanov, L. Litov, B. Pavlov, P. Petkov, A. Petrov

Beihang University, Beijing, China

T. Cheng, Q. Guo, T. Javaid[6], M. Mittal, H. Wang, L. Yuan

Department of Physics, Tsinghua University, Beijing, China

M. Ahmad, G. Bauer, C. Dozen[7], Z. Hu, J. Martins[8], Y. Wang, K. Yi[9,10]

Institute of High Energy Physics, Beijing, China

E. Chapon, G.M. Chen[6], H.S. Chen[6], M. Chen, F. Iemmi, A. Kapoor, D. Leggat, H. Liao, Z.-A. Liu[6], V. Milosevic, F. Monti, R. Sharma, J. Tao, J. Thomas-Wilsker, J. Wang, H. Zhang, S. Zhang[6], J. Zhao

State Key Laboratory of Nuclear Physics and Technology, Peking University, Beijing, China

A. Agapitos, Y. An, Y. Ban, C. Chen, A. Levin, Q. Li, X. Lyu, Y. Mao, S.J. Qian, D. Wang, Q. Wang, J. Xiao

Sun Yat-Sen University, Guangzhou, China

M. Lu, Z. You

Institute of Modern Physics and Key Laboratory of Nuclear Physics and Ion-beam Application (MOE) — Fudan University, Shanghai, China

X. Gao[3], H. Okawa

Zhejiang University, Hangzhou, China

Z. Lin, M. Xiao

Universidad de Los Andes, Bogota, Colombia

C. Avila, A. Cabrera, C. Florez, J. Fraga, A. Sarkar, M.A. Segura Delgado

Universidad de Antioquia, Medellin, Colombia

J. Mejia Guisao, F. Ramirez, J.D. Ruiz Alvarez, C.A. Salazar González

University of Split, Faculty of Electrical Engineering, Mechanical Engineering and Naval Architecture, Split, Croatia

D. Giljanovic, N. Godinovic, D. Lelas, I. Puljak

JHEP11(2021)057

University of Split, Faculty of Science, Split, Croatia
Z. Antunovic, M. Kovac, T. Sculac

Institute Rudjer Boskovic, Zagreb, Croatia
V. Brigljevic, D. Ferencek, D. Majumder, M. Roguljic, A. Starodumov[11], T. Susa

University of Cyprus, Nicosia, Cyprus
A. Attikis, K. Christoforou, E. Erodotou, A. Ioannou, G. Kole, M. Kolosova, S. Konstantinou, J. Mousa, C. Nicolaou, F. Ptochos, P.A. Razis, H. Rykaczewski, H. Saka

Charles University, Prague, Czech Republic
M. Finger[12], M. Finger Jr.[12], A. Kveton

Escuela Politecnica Nacional, Quito, Ecuador
E. Ayala

Universidad San Francisco de Quito, Quito, Ecuador
E. Carrera Jarrin

Academy of Scientific Research and Technology of the Arab Republic of Egypt, Egyptian Network of High Energy Physics, Cairo, Egypt
H. Abdalla[13], A.A. Abdelalim[14,15]

Center for High Energy Physics (CHEP-FU), Fayoum University, El-Fayoum, Egypt
M.A. Mahmoud, Y. Mohammed

National Institute of Chemical Physics and Biophysics, Tallinn, Estonia
S. Bhowmik, R.K. Dewanjee, K. Ehataht, M. Kadastik, S. Nandan, C. Nielsen, J. Pata, M. Raidal, L. Tani, C. Veelken

Department of Physics, University of Helsinki, Helsinki, Finland
P. Eerola, L. Forthomme, H. Kirschenmann, K. Osterberg, M. Voutilainen

Helsinki Institute of Physics, Helsinki, Finland
S. Bharthuar, E. Brücken, F. Garcia, J. Havukainen, M.S. Kim, R. Kinnunen, T. Lampén, K. Lassila-Perini, S. Lehti, T. Lindén, M. Lotti, L. Martikainen, M. Myllymäki, J. Ott, H. Siikonen, E. Tuominen, J. Tuominiemi

Lappeenranta University of Technology, Lappeenranta, Finland
P. Luukka, H. Petrow, T. Tuuva

IRFU, CEA, Université Paris-Saclay, Gif-sur-Yvette, France
C. Amendola, M. Besancon, F. Couderc, M. Dejardin, D. Denegri, J.L. Faure, F. Ferri, S. Ganjour, A. Givernaud, P. Gras, G. Hamel de Monchenault, P. Jarry, B. Lenzi, E. Locci, J. Malcles, J. Rander, A. Rosowsky, M.Ö. Sahin, A. Savoy-Navarro[16], M. Titov, G.B. Yu

Laboratoire Leprince-Ringuet, CNRS/IN2P3, Ecole Polytechnique, Institut Polytechnique de Paris, Palaiseau, France
S. Ahuja, F. Beaudette, M. Bonanomi, A. Buchot Perraguin, P. Busson, A. Cappati, C. Charlot, O. Davignon, B. Diab, G. Falmagne, S. Ghosh, R. Granier de Cassagnac,

JHEP11(2021)057

A. Hakimi, I. Kucher, J. Motta, M. Nguyen, C. Ochando, P. Paganini, J. Rembser, R. Salerno, J.B. Sauvan, Y. Sirois, A. Tarabini, A. Zabi, A. Zghiche

Université de Strasbourg, CNRS, IPHC UMR 7178, Strasbourg, France

J.-L. Agram[17], J. Andrea, D. Apparu, D. Bloch, G. Bourgatte, J.-M. Brom, E.C. Chabert, C. Collard, D. Darej, J.-C. Fontaine[17], U. Goerlach, C. Grimault, A.-C. Le Bihan, E. Nibigira, P. Van Hove

Institut de Physique des 2 Infinis de Lyon (IP2I), Villeurbanne, France

E. Asilar, S. Beauceron, C. Bernet, G. Boudoul, C. Camen, A. Carle, N. Chanon, D. Contardo, P. Depasse, H. El Mamouni, J. Fay, S. Gascon, M. Gouzevitch, B. Ille, I.B. Laktineh, H. Lattaud, A. Lesauvage, M. Lethuillier, L. Mirabito, S. Perries, K. Shchablo, V. Sordini, L. Torterotot, G. Touquet, M. Vander Donckt, S. Viret

Georgian Technical University, Tbilisi, Georgia

A. Khvedelidze[12], I. Lomidze, Z. Tsamalaidze[12]

RWTH Aachen University, I. Physikalisches Institut, Aachen, Germany

L. Feld, K. Klein, M. Lipinski, D. Meuser, A. Pauls, M.P. Rauch, N. Röwert, J. Schulz, M. Teroerde

RWTH Aachen University, III. Physikalisches Institut A, Aachen, Germany

A. Dodonova, D. Eliseev, M. Erdmann, P. Fackeldey, B. Fischer, S. Ghosh, T. Hebbeker, K. Hoepfner, F. Ivone, H. Keller, L. Mastrolorenzo, M. Merschmeyer, A. Meyer, G. Mocellin, S. Mondal, S. Mukherjee, D. Noll, A. Novak, T. Pook, A. Pozdnyakov, Y. Rath, H. Reithler, J. Roemer, A. Schmidt, S.C. Schuler, A. Sharma, L. Vigilante, S. Wiedenbeck, S. Zaleski

RWTH Aachen University, III. Physikalisches Institut B, Aachen, Germany

C. Dziwok, G. Flügge, W. Haj Ahmad[18], O. Hlushchenko, T. Kress, A. Nowack, C. Pistone, O. Pooth, D. Roy, H. Sert, A. Stahl[19], T. Ziemons

Deutsches Elektronen-Synchrotron, Hamburg, Germany

H. Aarup Petersen, M. Aldaya Martin, P. Asmuss, I. Babounikau, S. Baxter, O. Behnke, A. Bermúdez Martínez, S. Bhattacharya, A.A. Bin Anuar, K. Borras[20], V. Botta, D. Brunner, A. Campbell, A. Cardini, C. Cheng, F. Colombina, S. Consuegra Rodríguez, G. Correia Silva, V. Danilov, L. Didukh, G. Eckerlin, D. Eckstein, L.I. Estevez Banos, O. Filatov, E. Gallo[21], A. Geiser, A. Giraldi, A. Grohsjean, M. Guthoff, A. Jafari[22], N.Z. Jomhari, H. Jung, A. Kasem[20], M. Kasemann, H. Kaveh, C. Kleinwort, D. Krücker, W. Lange, J. Lidrych, K. Lipka, W. Lohmann[23], R. Mankel, I.-A. Melzer-Pellmann, M. Mendizabal Morentin, J. Metwally, A.B. Meyer, M. Meyer, J. Mnich, A. Mussgiller, Y. Otarid, D. Pérez Adán, D. Pitzl, A. Raspereza, B. Ribeiro Lopes, J. Rübenach, A. Saggio, A. Saibel, M. Savitskyi, M. Scham, V. Scheurer, P. Schütze, C. Schwanenberger[21], A. Singh, R.E. Sosa Ricardo, D. Stafford, N. Tonon, O. Turkot, M. Van De Klundert, R. Walsh, D. Walter, Y. Wen, K. Wichmann, L. Wiens, C. Wissing, S. Wuchterl

JHEP11(2021)057

University of Hamburg, Hamburg, Germany

R. Aggleton, S. Albrecht, S. Bein, L. Benato, A. Benecke, P. Connor, K. De Leo, M. Eich, F. Feindt, A. Fröhlich, C. Garbers, E. Garutti, P. Gunnellini, J. Haller, A. Hinzmann, G. Kasieczka, R. Klanner, R. Kogler, T. Kramer, V. Kutzner, J. Lange, T. Lange, A. Lobanov, A. Malara, A. Nigamova, K.J. Pena Rodriguez, O. Rieger, P. Schleper, M. Schröder, J. Schwandt, D. Schwarz, J. Sonneveld, H. Stadie, G. Steinbrück, A. Tews, B. Vormwald, I. Zoi

Karlsruher Institut fuer Technologie, Karlsruhe, Germany

J. Bechtel, T. Berger, E. Butz, R. Caspart, T. Chwalek, W. De Boer†, A. Dierlamm, A. Droll, K. El Morabit, N. Faltermann, M. Giffels, J.-O. Gosewisch, A. Gottmann, F. Hartmann[19], C. Heidecker, U. Husemann, I. Katkov[24], P. Keicher, R. Koppenhöfer, S. Maier, M. Metzler, S. Mitra, Th. Müller, M. Neukum, A. Nürnberg, G. Quast, K. Rabbertz, J. Rauser, D. Savoiu, M. Schnepf, D. Seith, I. Shvetsov, H.J. Simonis, R. Ulrich, J. Van Der Linden, R.F. Von Cube, M. Wassmer, M. Weber, S. Wieland, R. Wolf, S. Wozniewski, S. Wunsch

Institute of Nuclear and Particle Physics (INPP), NCSR Demokritos, Aghia Paraskevi, Greece

G. Anagnostou, G. Daskalakis, T. Geralis, A. Kyriakis, D. Loukas, A. Stakia

National and Kapodistrian University of Athens, Athens, Greece

M. Diamantopoulou, D. Karasavvas, G. Karathanasis, P. Kontaxakis, C.K. Koraka, A. Manousakis-Katsikakis, A. Panagiotou, I. Papavergou, N. Saoulidou, K. Theofilatos, E. Tziaferi, K. Vellidis, E. Vourliotis

National Technical University of Athens, Athens, Greece

G. Bakas, K. Kousouris, I. Papakrivopoulos, G. Tsipolitis, A. Zacharopoulou

University of Ioánnina, Ioánnina, Greece

I. Evangelou, C. Foudas, P. Gianneios, P. Katsoulis, P. Kokkas, N. Manthos, I. Papadopoulos, J. Strologas

MTA-ELTE Lendület CMS Particle and Nuclear Physics Group, Eötvös Loránd University, Budapest, Hungary

M. Csanad, K. Farkas, M.M.A. Gadallah[25], S. Lökös[26], P. Major, K. Mandal, A. Mehta, G. Pasztor, A.J. Rádl, O. Surányi, G.I. Veres

Wigner Research Centre for Physics, Budapest, Hungary

M. Bartók[27], G. Bencze, C. Hajdu, D. Horvath[28], F. Sikler, V. Veszpremi, G. Vesztergombi†

Institute of Nuclear Research ATOMKI, Debrecen, Hungary

S. Czellar, J. Karancsi[27], J. Molnar, Z. Szillasi, D. Teyssier

Institute of Physics, University of Debrecen, Debrecen, Hungary

P. Raics, Z.L. Trocsanyi[29], G. Zilizi

Karoly Robert Campus, MATE Institute of Technology

T. Csorgo[30], F. Nemes[30], T. Novak

JHEP11(2021)057

Indian Institute of Science (IISc), Bangalore, India

J.R. Komaragiri, D. Kumar, L. Panwar, P.C. Tiwari

National Institute of Science Education and Research, HBNI, Bhubaneswar, India

S. Bahinipati[31], C. Kar, P. Mal, T. Mishra, V.K. Muraleedharan Nair Bindhu[32], A. Nayak[32], P. Saha, N. Sur, S.K. Swain, D. Vats[32]

Panjab University, Chandigarh, India

S. Bansal, S.B. Beri, V. Bhatnagar, G. Chaudhary, S. Chauhan, N. Dhingra[33], R. Gupta, A. Kaur, M. Kaur, S. Kaur, P. Kumari, M. Meena, K. Sandeep, J.B. Singh, A.K. Virdi

University of Delhi, Delhi, India

A. Ahmed, A. Bhardwaj, B.C. Choudhary, M. Gola, S. Keshri, A. Kumar, M. Naimuddin, P. Priyanka, K. Ranjan, A. Shah

Saha Institute of Nuclear Physics, HBNI, Kolkata, India

M. Bharti[34], R. Bhattacharya, S. Bhattacharya, D. Bhowmik, S. Dutta, S. Dutta, B. Gomber[35], M. Maity[36], P. Palit, P.K. Rout, G. Saha, B. Sahu, S. Sarkar, M. Sharan, B. Singh[34], S. Thakur[34]

Indian Institute of Technology Madras, Madras, India

P.K. Behera, S.C. Behera, P. Kalbhor, A. Muhammad, R. Pradhan, P.R. Pujahari, A. Sharma, A.K. Sikdar

Bhabha Atomic Research Centre, Mumbai, India

D. Dutta, V. Jha, V. Kumar, D.K. Mishra, K. Naskar[37], P.K. Netrakanti, L.M. Pant, P. Shukla

Tata Institute of Fundamental Research-A, Mumbai, India

T. Aziz, S. Dugad, M. Kumar, U. Sarkar

Tata Institute of Fundamental Research-B, Mumbai, India

S. Banerjee, R. Chudasama, M. Guchait, S. Karmakar, S. Kumar, G. Majumder, K. Mazumdar, S. Mukherjee

Indian Institute of Science Education and Research (IISER), Pune, India

K. Alpana, S. Dube, B. Kansal, A. Laha, S. Pandey, A. Rane, A. Rastogi, S. Sharma

Department of Physics, Isfahan University of Technology, Isfahan, Iran

H. Bakhshiansohi[38], M. Zeinali[39]

Institute for Research in Fundamental Sciences (IPM), Tehran, Iran

S. Chenarani[40], S.M. Etesami, M. Khakzad, M. Mohammadi Najafabadi

University College Dublin, Dublin, Ireland

M. Grunewald

JHEP11(2021)057

INFN Sezione di Bari [a], Università di Bari [b], Politecnico di Bari [c], Bari, Italy
M. Abbrescia[a,b], R. Aly[a,b,41], C. Aruta[a,b], A. Colaleo[a], D. Creanza[a,c], N. De Filippis[a,c], M. De Palma[a,b], A. Di Florio[a,b], A. Di Pilato[a,b], W. Elmetenawee[a,b], L. Fiore[a], A. Gelmi[a,b], M. Gul[a], G. Iaselli[a,c], M. Ince[a,b], S. Lezki[a,b], G. Maggi[a,c], M. Maggi[a], I. Margjeka[a,b], V. Mastrapasqua[a,b], J.A. Merlin[a], S. My[a,b], S. Nuzzo[a,b], A. Pellecchia[a,b], A. Pompili[a,b], G. Pugliese[a,c], A. Ranieri[a], G. Selvaggi[a,b], L. Silvestris[a], F.M. Simone[a,b], R. Venditti[a], P. Verwilligen[a]

INFN Sezione di Bologna [a], Università di Bologna [b], Bologna, Italy
G. Abbiendi[a], C. Battilana[a,b], D. Bonacorsi[a,b], L. Borgonovi[a], L. Brigliadori[a], R. Campanini[a,b], P. Capiluppi[a,b], A. Castro[a,b], F.R. Cavallo[a], M. Cuffiani[a,b], G.M. Dallavalle[a], T. Diotalevi[a,b], F. Fabbri[a], A. Fanfani[a,b], P. Giacomelli[a], L. Giommi[a,b], C. Grandi[a], L. Guiducci[a,b], S. Lo Meo[a,42], L. Lunerti[a,b], S. Marcellini[a], G. Masetti[a], F.L. Navarria[a,b], A. Perrotta[a], F. Primavera[a,b], A.M. Rossi[a,b], T. Rovelli[a,b], G.P. Siroli[a,b]

INFN Sezione di Catania [a], Università di Catania [b], Catania, Italy
S. Albergo[a,b,43], S. Costa[a,b,43], A. Di Mattia[a], R. Potenza[a,b], A. Tricomi[a,b,43], C. Tuve[a,b]

INFN Sezione di Firenze [a], Università di Firenze [b], Firenze, Italy
G. Barbagli[a], A. Cassese[a], R. Ceccarelli[a,b], V. Ciulli[a,b], C. Civinini[a], R. D'Alessandro[a,b], E. Focardi[a,b], G. Latino[a,b], P. Lenzi[a,b], M. Lizzo[a,b], M. Meschini[a], S. Paoletti[a], R. Seidita[a,b], G. Sguazzoni[a], L. Viliani[a]

INFN Laboratori Nazionali di Frascati, Frascati, Italy
L. Benussi, S. Bianco, D. Piccolo

INFN Sezione di Genova [a], Università di Genova [b], Genova, Italy
M. Bozzo[a,b], F. Ferro[a], R. Mulargia[a,b], E. Robutti[a], S. Tosi[a,b]

INFN Sezione di Milano-Bicocca [a], Università di Milano-Bicocca [b], Milano, Italy
A. Benaglia[a], F. Brivio[a,b], F. Cetorelli[a,b], V. Ciriolo[a,b,19], F. De Guio[a,b], M.E. Dinardo[a,b], P. Dini[a], S. Gennai[a], A. Ghezzi[a,b], P. Govoni[a,b], L. Guzzi[a,b], M. Malberti[a], S. Malvezzi[a], A. Massironi[a], D. Menasce[a], L. Moroni[a], M. Paganoni[a,b], D. Pedrini[a], S. Ragazzi[a,b], N. Redaelli[a], T. Tabarelli de Fatis[a,b], D. Valsecchi[a,b,19], D. Zuolo[a,b]

INFN Sezione di Napoli [a], Università di Napoli 'Federico II' [b], Napoli, Italy, Università della Basilicata [c], Potenza, Italy, Università G. Marconi [d], Roma, Italy
S. Buontempo[a], F. Carnevali[a,b], N. Cavallo[a,c], A. De Iorio[a,b], F. Fabozzi[a,c], A.O.M. Iorio[a,b], L. Lista[a,b], S. Meola[a,d,19], P. Paolucci[a,19], B. Rossi[a], C. Sciacca[a,b]

INFN Sezione di Padova [a], Università di Padova [b], Padova, Italy, Università di Trento [c], Trento, Italy
P. Azzi[a], N. Bacchetta[a], D. Bisello[a,b], P. Bortignon[a], A. Bragagnolo[a,b], R. Carlin[a,b], P. Checchia[a], T. Dorigo[a], U. Dosselli[a], F. Gasparini[a,b], U. Gasparini[a,b], S.Y. Hoh[a,b], L. Layer[a,44], M. Margoni[a,b], A.T. Meneguzzo[a,b], J. Pazzini[a,b], M. Presilla[a,b],

JHEP11(2021)057

P. Ronchese[a,b], R. Rossin[a,b], F. Simonetto[a,b], G. Strong[a], M. Tosi[a,b], H. YARAR[a,b], M. Zanetti[a,b], P. Zotto[a,b], A. Zucchetta[a,b], G. Zumerle[a,b]

INFN Sezione di Pavia [a], Università di Pavia [b], Pavia, Italy

C. Aime'[a,b], A. Braghieri[a], S. Calzaferri[a,b], D. Fiorina[a,b], P. Montagna[a,b], S.P. Ratti[a,b], V. Re[a], C. Riccardi[a,b], P. Salvini[a], I. Vai[a], P. Vitulo[a,b]

INFN Sezione di Perugia [a], Università di Perugia [b], Perugia, Italy

P. Asenov[a,45], G.M. Bilei[a], D. Ciangottini[a,b], L. Fanò[a,b], P. Lariccia[a,b], M. Magherini[b], G. Mantovani[a,b], V. Mariani[a,b], M. Menichelli[a], F. Moscatelli[a,45], A. Piccinelli[a,b], A. Rossi[a,b], A. Santocchia[a,b], D. Spiga[a], T. Tedeschi[a,b]

INFN Sezione di Pisa [a], Università di Pisa [b], Scuola Normale Superiore di Pisa [c], Pisa Italy, Università di Siena [d], Siena, Italy

P. Azzurri[a], G. Bagliesi[a], V. Bertacchi[a,c], L. Bianchini[a], T. Boccali[a], E. Bossini[a,b], R. Castaldi[a], M.A. Ciocci[a,b], V. D'Amante[a,d], R. Dell'Orso[a], M.R. Di Domenico[a,d], S. Donato[a], A. Giassi[a], F. Ligabue[a,c], E. Manca[a,c], G. Mandorli[a,c], A. Messineo[a,b], F. Palla[a], S. Parolia[a,b], G. Ramirez-Sanchez[a,c], A. Rizzi[a,b], G. Rolandi[a,c], S. Roy Chowdhury[a,c], A. Scribano[a], N. Shafiei[a,b], P. Spagnolo[a], R. Tenchini[a], G. Tonelli[a,b], N. Turini[a,d], A. Venturi[a], P.G. Verdini[a]

INFN Sezione di Roma [a], Sapienza Università di Roma [b], Rome, Italy

M. Campana[a,b], F. Cavallari[a], D. Del Re[a,b], E. Di Marco[a], M. Diemoz[a], E. Longo[a,b], P. Meridiani[a], G. Organtini[a,b], F. Pandolfi[a], R. Paramatti[a,b], C. Quaranta[a,b], S. Rahatlou[a,b], C. Rovelli[a], F. Santanastasio[a,b], L. Soffi[a], R. Tramontano[a,b]

INFN Sezione di Torino [a], Università di Torino [b], Torino, Italy, Università del Piemonte Orientale [c], Novara, Italy

N. Amapane[a,b], R. Arcidiacono[a,c], S. Argiro[a,b], M. Arneodo[a,c], N. Bartosik[a], R. Bellan[a,b], A. Bellora[a,b], J. Berenguer Antequera[a,b], C. Biino[a], N. Cartiglia[a], S. Cometti[a], M. Costa[a,b], R. Covarelli[a,b], N. Demaria[a], B. Kiani[a,b], F. Legger[a], C. Mariotti[a], S. Maselli[a], E. Migliore[a,b], E. Monteil[a,b], M. Monteno[a], M.M. Obertino[a,b], G. Ortona[a], L. Pacher[a,b], N. Pastrone[a], M. Pelliccioni[a], G.L. Pinna Angioni[a,b], M. Ruspa[a,c], K. Shchelina[a,b], F. Siviero[a,b], V. Sola[a], A. Solano[a,b], D. Soldi[a,b], A. Staiano[a], M. Tornago[a,b], D. Trocino[a,b], A. Vagnerini

INFN Sezione di Trieste [a], Università di Trieste [b], Trieste, Italy

S. Belforte[a], V. Candelise[a,b], M. Casarsa[a], F. Cossutti[a], A. Da Rold[a,b], G. Della Ricca[a,b], G. Sorrentino[a,b], F. Vazzoler[a,b]

Kyungpook National University, Daegu, Korea

S. Dogra, C. Huh, B. Kim, D.H. Kim, G.N. Kim, J. Kim, J. Lee, S.W. Lee, C.S. Moon, Y.D. Oh, S.I. Pak, B.C. Radburn-Smith, S. Sekmen, Y.C. Yang

Chonnam National University, Institute for Universe and Elementary Particles, Kwangju, Korea

H. Kim, D.H. Moon

JHEP11(2021)057

Hanyang University, Seoul, Korea
B. Francois, T.J. Kim, J. Park

Korea University, Seoul, Korea
S. Cho, S. Choi, Y. Go, B. Hong, K. Lee, K.S. Lee, J. Lim, J. Park, S.K. Park, J. Yoo

Kyung Hee University, Department of Physics, Seoul, Republic of Korea
J. Goh, A. Gurtu

Sejong University, Seoul, Korea
H.S. Kim, Y. Kim

Seoul National University, Seoul, Korea
J. Almond, J.H. Bhyun, J. Choi, S. Jeon, J. Kim, J.S. Kim, S. Ko, H. Kwon, H. Lee, S. Lee, B.H. Oh, M. Oh, S.B. Oh, H. Seo, U.K. Yang, I. Yoon

University of Seoul, Seoul, Korea
W. Jang, D. Jeon, D.Y. Kang, Y. Kang, J.H. Kim, S. Kim, B. Ko, J.S.H. Lee, Y. Lee, I.C. Park, Y. Roh, M.S. Ryu, D. Song, I.J. Watson, S. Yang

Yonsei University, Department of Physics, Seoul, Korea
S. Ha, H.D. Yoo

Sungkyunkwan University, Suwon, Korea
M. Choi, Y. Jeong, H. Lee, Y. Lee, I. Yu

College of Engineering and Technology, American University of the Middle East (AUM), Egaila, Kuwait
T. Beyrouthy, Y. Maghrbi

Riga Technical University, Riga, Latvia
T. Torims, V. Veckalns[46]

Vilnius University, Vilnius, Lithuania
M. Ambrozas, A. Carvalho Antunes De Oliveira, A. Juodagalvis, A. Rinkevicius, G. Tamulaitis

National Centre for Particle Physics, Universiti Malaya, Kuala Lumpur, Malaysia
N. Bin Norjoharuddeen, W.A.T. Wan Abdullah, M.N. Yusli, Z. Zolkapli

Universidad de Sonora (UNISON), Hermosillo, Mexico
J.F. Benitez, A. Castaneda Hernandez, M. León Coello, J.A. Murillo Quijada, A. Sehrawat, L. Valencia Palomo

Centro de Investigacion y de Estudios Avanzados del IPN, Mexico City, Mexico
G. Ayala, H. Castilla-Valdez, E. De La Cruz-Burelo, I. Heredia-De La Cruz[47], R. Lopez-Fernandez, C.A. Mondragon Herrera, D.A. Perez Navarro, A. Sanchez-Hernandez

Universidad Iberoamericana, Mexico City, Mexico
S. Carrillo Moreno, C. Oropeza Barrera, F. Vazquez Valencia

JHEP11(2021)057

Benemerita Universidad Autonoma de Puebla, Puebla, Mexico
I. Pedraza, H.A. Salazar Ibarguen, C. Uribe Estrada

University of Montenegro, Podgorica, Montenegro
J. Mijuskovic[48], N. Raicevic

University of Auckland, Auckland, New Zealand
D. Krofcheck

University of Canterbury, Christchurch, New Zealand
S. Bheesette, P.H. Butler

National Centre for Physics, Quaid-I-Azam University, Islamabad, Pakistan
A. Ahmad, M.I. Asghar, A. Awais, M.I.M. Awan, H.R. Hoorani, W.A. Khan, M.A. Shah, M. Shoaib, M. Waqas

AGH University of Science and Technology Faculty of Computer Science, Electronics and Telecommunications, Krakow, Poland
V. Avati, L. Grzanka, M. Malawski

National Centre for Nuclear Research, Swierk, Poland
H. Bialkowska, M. Bluj, B. Boimska, M. Górski, M. Kazana, M. Szleper, P. Zalewski

Institute of Experimental Physics, Faculty of Physics, University of Warsaw, Warsaw, Poland
K. Bunkowski, K. Doroba, A. Kalinowski, M. Konecki, J. Krolikowski, M. Walczak

Laboratório de Instrumentação e Física Experimental de Partículas, Lisboa, Portugal
M. Araujo, P. Bargassa, D. Bastos, A. Boletti, P. Faccioli, M. Gallinaro, J. Hollar, N. Leonardo, T. Niknejad, M. Pisano, J. Seixas, O. Toldaiev, J. Varela

Joint Institute for Nuclear Research, Dubna, Russia
S. Afanasiev, D. Budkouski, I. Golutvin, I. Gorbunov, V. Karjavine, V. Korenkov, A. Lanev, A. Malakhov, V. Matveev[49,50], V. Palichik, V. Perelygin, M. Savina, D. Seitova, V. Shalaev, S. Shmatov, S. Shulha, V. Smirnov, O. Teryaev, N. Voytishin, B.S. Yuldashev[51], A. Zarubin, I. Zhizhin

Petersburg Nuclear Physics Institute, Gatchina (St. Petersburg), Russia
G. Gavrilov, V. Golovtcov, Y. Ivanov, V. Kim[52], E. Kuznetsova[53], V. Murzin, V. Oreshkin, I. Smirnov, D. Sosnov, V. Sulimov, L. Uvarov, S. Volkov, A. Vorobyev

Institute for Nuclear Research, Moscow, Russia
Yu. Andreev, A. Dermenev, S. Gninenko, N. Golubev, A. Karneyeu, D. Kirpichnikov, M. Kirsanov, N. Krasnikov, A. Pashenkov, G. Pivovarov, D. Tlisov†, A. Toropin

Institute for Theoretical and Experimental Physics named by A.I. Alikhanov of NRC 'Kurchatov Institute', Moscow, Russia
V. Epshteyn, V. Gavrilov, N. Lychkovskaya, A. Nikitenko[54], V. Popov, A. Spiridonov, A. Stepennov, M. Toms, E. Vlasov, A. Zhokin

JHEP11(2021)057

Moscow Institute of Physics and Technology, Moscow, Russia

T. Aushev

National Research Nuclear University 'Moscow Engineering Physics Institute' (MEPhI), Moscow, Russia

O. Bychkova, R. Chistov[55], M. Danilov[56], A. Oskin, S. Polikarpov[56]

P.N. Lebedev Physical Institute, Moscow, Russia

V. Andreev, M. Azarkin, I. Dremin, M. Kirakosyan, A. Terkulov

Skobeltsyn Institute of Nuclear Physics, Lomonosov Moscow State University, Moscow, Russia

A. Belyaev, E. Boos, V. Bunichev, M. Dubinin[57], L. Dudko, A. Ershov, A. Gribushin, V. Klyukhin, O. Kodolova, I. Lokhtin, S. Obraztsov, S. Petrushanko, V. Savrin

Novosibirsk State University (NSU), Novosibirsk, Russia

V. Blinov[58], T. Dimova[58], L. Kardapoltsev[58], A. Kozyrev[58], I. Ovtin[58], Y. Skovpen[58]

Institute for High Energy Physics of National Research Centre 'Kurchatov Institute', Protvino, Russia

I. Azhgirey, I. Bayshev, D. Elumakhov, V. Kachanov, D. Konstantinov, P. Mandrik, V. Petrov, R. Ryutin, S. Slabospitskii, A. Sobol, S. Troshin, N. Tyurin, A. Uzunian, A. Volkov

National Research Tomsk Polytechnic University, Tomsk, Russia

A. Babaev, V. Okhotnikov

Tomsk State University, Tomsk, Russia

V. Borshch, V. Ivanchenko, E. Tcherniaev

University of Belgrade: Faculty of Physics and VINCA Institute of Nuclear Sciences, Belgrade, Serbia

P. Adzic[59], M. Dordevic, P. Milenovic, J. Milosevic

Centro de Investigaciones Energéticas Medioambientales y Tecnológicas (CIEMAT), Madrid, Spain

M. Aguilar-Benitez, J. Alcaraz Maestre, A. Álvarez Fernández, I. Bachiller, M. Barrio Luna, Cristina F. Bedoya, C.A. Carrillo Montoya, M. Cepeda, M. Cerrada, N. Colino, B. De La Cruz, A. Delgado Peris, J.P. Fernández Ramos, J. Flix, M.C. Fouz, O. Gonzalez Lopez, S. Goy Lopez, J.M. Hernandez, M.I. Josa, J. León Holgado, D. Moran, Á. Navarro Tobar, C. Perez Dengra, A. Pérez-Calero Yzquierdo, J. Puerta Pelayo, I. Redondo, L. Romero, S. Sánchez Navas, L. Urda Gómez, C. Willmott

Universidad Autónoma de Madrid, Madrid, Spain

J.F. de Trocóniz, R. Reyes-Almanza

JHEP11(2021)057

Universidad de Oviedo, Instituto Universitario de Ciencias y Tecnologías Espaciales de Asturias (ICTEA), Oviedo, Spain

B. Alvarez Gonzalez, J. Cuevas, C. Erice, J. Fernandez Menendez, S. Folgueras, I. Gonzalez Caballero, J.R. González Fernández, E. Palencia Cortezon, C. Ramón Álvarez, J. Ripoll Sau, V. Rodríguez Bouza, A. Trapote, N. Trevisani

Instituto de Física de Cantabria (IFCA), CSIC-Universidad de Cantabria, Santander, Spain

J.A. Brochero Cifuentes, I.J. Cabrillo, A. Calderon, J. Duarte Campderros, M. Fernandez, C. Fernandez Madrazo, P.J. Fernández Manteca, A. García Alonso, G. Gomez, C. Martinez Rivero, P. Martinez Ruiz del Arbol, F. Matorras, P. Matorras Cuevas, J. Piedra Gomez, C. Prieels, T. Rodrigo, A. Ruiz-Jimeno, L. Scodellaro, I. Vila, J.M. Vizan Garcia

University of Colombo, Colombo, Sri Lanka

M.K. Jayananda, B. Kailasapathy[60], D.U.J. Sonnadara, D.D.C. Wickramarathna

University of Ruhuna, Department of Physics, Matara, Sri Lanka

W.G.D. Dharmaratna, K. Liyanage, N. Perera, N. Wickramage

CERN, European Organization for Nuclear Research, Geneva, Switzerland

T.K. Aarrestad, D. Abbaneo, J. Alimena, E. Auffray, G. Auzinger, J. Baechler, P. Baillon[†], D. Barney, J. Bendavid, M. Bianco, A. Bocci, T. Camporesi, M. Capeans Garrido, G. Cerminara, S.S. Chhibra, M. Cipriani, L. Cristella, D. d'Enterria, A. Dabrowski, N. Daci, A. David, A. De Roeck, M.M. Defranchis, M. Deile, M. Dobson, M. Dünser, N. Dupont, A. Elliott-Peisert, N. Emriskova, F. Fallavollita[61], D. Fasanella, A. Florent, G. Franzoni, W. Funk, S. Giani, D. Gigi, K. Gill, F. Glege, L. Gouskos, M. Haranko, J. Hegeman, Y. Iiyama, V. Innocente, T. James, P. Janot, J. Kaspar, J. Kieseler, M. Komm, N. Kratochwil, C. Lange, S. Laurila, P. Lecoq, K. Long, C. Lourenço, L. Malgeri, S. Mallios, M. Mannelli, A.C. Marini, F. Meijers, S. Mersi, E. Meschi, F. Moortgat, M. Mulders, S. Orfanelli, L. Orsini, F. Pantaleo, L. Pape, E. Perez, M. Peruzzi, A. Petrilli, G. Petrucciani, A. Pfeiffer, M. Pierini, D. Piparo, M. Pitt, H. Qu, T. Quast, D. Rabady, A. Racz, G. Reales Gutiérrez, M. Rieger, M. Rovere, H. Sakulin, J. Salfeld-Nebgen, S. Scarfi, C. Schäfer, C. Schwick, M. Selvaggi, A. Sharma, P. Silva, W. Snoeys, P. Sphicas[62], S. Summers, K. Tatar, V.R. Tavolaro, D. Treille, A. Tsirou, G.P. Van Onsem, M. Verzetti, J. Wanczyk[63], K.A. Wozniak, W.D. Zeuner

Paul Scherrer Institut, Villigen, Switzerland

L. Caminada[64], A. Ebrahimi, W. Erdmann, R. Horisberger, Q. Ingram, H.C. Kaestli, D. Kotlinski, U. Langenegger, M. Missiroli, T. Rohe

ETH Zurich — Institute for Particle Physics and Astrophysics (IPA), Zurich, Switzerland

K. Androsov[63], M. Backhaus, P. Berger, A. Calandri, N. Chernyavskaya, A. De Cosa, G. Dissertori, M. Dittmar, M. Donegà, C. Dorfer, F. Eble, K. Gedia, F. Glessgen, T.A. Gómez Espinosa, C. Grab, D. Hits, W. Lustermann, A.-M. Lyon, R.A. Manzoni,

JHEP11(2021)057

C. Martin Perez, M.T. Meinhard, F. Nessi-Tedaldi, J. Niedziela, F. Pauss, V. Perovic, S. Pigazzini, M.G. Ratti, M. Reichmann, C. Reissel, T. Reitenspiess, B. Ristic, D. Ruini, D.A. Sanz Becerra, M. Schönenberger, V. Stampf, J. Steggemann[63], R. Wallny, D.H. Zhu

Universität Zürich, Zurich, Switzerland

C. Amsler[65], P. Bärtschi, C. Botta, D. Brzhechko, M.F. Canelli, K. Cormier, A. De Wit, R. Del Burgo, J.K. Heikkilä, M. Huwiler, W. Jin, A. Jofrehei, B. Kilminster, S. Leontsinis, S.P. Liechti, A. Macchiolo, P. Meiring, V.M. Mikuni, U. Molinatti, I. Neutelings, A. Reimers, P. Robmann, S. Sanchez Cruz, K. Schweiger, Y. Takahashi

National Central University, Chung-Li, Taiwan

C. Adloff[66], C.M. Kuo, W. Lin, A. Roy, T. Sarkar[36], S.S. Yu

National Taiwan University (NTU), Taipei, Taiwan

L. Ceard, Y. Chao, K.F. Chen, P.H. Chen, W.-S. Hou, Y.y. Li, R.-S. Lu, E. Paganis, A. Psallidas, A. Steen, H.y. Wu, E. Yazgan, P.r. Yu

Chulalongkorn University, Faculty of Science, Department of Physics, Bangkok, Thailand

B. Asavapibhop, C. Asawatangtrakuldee, N. Srimanobhas

Çukurova University, Physics Department, Science and Art Faculty, Adana, Turkey

F. Boran, S. Damarseckin[67], Z.S. Demiroglu, F. Dolek, I. Dumanoglu[68], E. Eskut, Y. Guler, E. Gurpinar Guler[69], I. Hos[70], C. Isik, O. Kara, A. Kayis Topaksu, U. Kiminsu, G. Onengut, K. Ozdemir[71], A. Polatoz, A.E. Simsek, B. Tali[72], U.G. Tok, S. Turkcapar, I.S. Zorbakir, C. Zorbilmez

Middle East Technical University, Physics Department, Ankara, Turkey

B. Isildak[73], G. Karapinar[74], K. Ocalan[75], M. Yalvac[76]

Bogazici University, Istanbul, Turkey

B. Akgun, I.O. Atakisi, E. Gülmez, M. Kaya[77], O. Kaya[78], Ö. Özçelik, S. Tekten[79], E.A. Yetkin[80]

Istanbul Technical University, Istanbul, Turkey

A. Cakir, K. Cankocak[68], Y. Komurcu, S. Sen[81]

Istanbul University, Istanbul, Turkey

S. Cerci[72], B. Kaynak, S. Ozkorucuklu, D. Sunar Cerci[72]

Institute for Scintillation Materials of National Academy of Science of Ukraine, Kharkov, Ukraine

B. Grynyov

National Scientific Center, Kharkov Institute of Physics and Technology, Kharkov, Ukraine

L. Levchuk

JHEP11(2021)057

University of Bristol, Bristol, United Kingdom

D. Anthony, E. Bhal, S. Bologna, J.J. Brooke, A. Bundock, E. Clement, D. Cussans, H. Flacher, J. Goldstein, G.P. Heath, H.F. Heath, M.l. Holmberg[82], L. Kreczko, B. Krikler, S. Paramesvaran, S. Seif El Nasr-Storey, V.J. Smith, N. Stylianou[83], K. Walkingshaw Pass, R. White

Rutherford Appleton Laboratory, Didcot, United Kingdom

K.W. Bell, A. Belyaev[84], C. Brew, R.M. Brown, D.J.A. Cockerill, C. Cooke, K.V. Ellis, K. Harder, S. Harper, J. Linacre, K. Manolopoulos, D.M. Newbold, E. Olaiya, D. Petyt, T. Reis, T. Schuh, C.H. Shepherd-Themistocleous, I.R. Tomalin, T. Williams

Imperial College, London, United Kingdom

R. Bainbridge, P. Bloch, S. Bonomally, J. Borg, S. Breeze, O. Buchmuller, V. Cepaitis, G.S. Chahal[85], D. Colling, P. Dauncey, G. Davies, M. Della Negra, S. Fayer, G. Fedi, G. Hall, M.H. Hassanshahi, G. Iles, J. Langford, L. Lyons, A.-M. Magnan, S. Malik, A. Martelli, D.G. Monk, J. Nash[86], M. Pesaresi, D.M. Raymond, A. Richards, A. Rose, E. Scott, C. Seez, A. Shtipliyski, A. Tapper, K. Uchida, T. Virdee[19], M. Vojinovic, N. Wardle, S.N. Webb, D. Winterbottom, A.G. Zecchinelli

Brunel University, Uxbridge, United Kingdom

K. Coldham, J.E. Cole, A. Khan, P. Kyberd, I.D. Reid, L. Teodorescu, S. Zahid

Baylor University, Waco, U.S.A.

S. Abdullin, A. Brinkerhoff, B. Caraway, J. Dittmann, K. Hatakeyama, A.R. Kanuganti, B. McMaster, N. Pastika, M. Saunders, S. Sawant, C. Sutantawibul, J. Wilson

Catholic University of America, Washington, DC, U.S.A.

R. Bartek, A. Dominguez, R. Uniyal, A.M. Vargas Hernandez

The University of Alabama, Tuscaloosa, U.S.A.

A. Buccilli, S.I. Cooper, D. Di Croce, S.V. Gleyzer, C. Henderson, C.U. Perez, P. Rumerio[87], C. West

Boston University, Boston, U.S.A.

A. Akpinar, A. Albert, D. Arcaro, C. Cosby, Z. Demiragli, E. Fontanesi, D. Gastler, J. Rohlf, K. Salyer, D. Sperka, D. Spitzbart, I. Suarez, A. Tsatsos, S. Yuan, D. Zou

Brown University, Providence, U.S.A.

G. Benelli, B. Burkle, X. Coubez[20], D. Cutts, M. Hadley, U. Heintz, J.M. Hogan[88], G. Landsberg, K.T. Lau, M. Lukasik, J. Luo, M. Narain, S. Sagir[89], E. Usai, W.Y. Wong, X. Yan, D. Yu, W. Zhang

University of California, Davis, Davis, U.S.A.

J. Bonilla, C. Brainerd, R. Breedon, M. Calderon De La Barca Sanchez, M. Chertok, J. Conway, P.T. Cox, R. Erbacher, G. Haza, F. Jensen, O. Kukral, R. Lander, M. Mulhearn, D. Pellett, B. Regnery, D. Taylor, Y. Yao, F. Zhang

JHEP11(2021)057

University of California, Los Angeles, U.S.A.

M. Bachtis, R. Cousins, A. Datta, D. Hamilton, J. Hauser, M. Ignatenko, M.A. Iqbal, T. Lam, W.A. Nash, S. Regnard, D. Saltzberg, B. Stone, V. Valuev

University of California, Riverside, Riverside, U.S.A.

K. Burt, Y. Chen, R. Clare, J.W. Gary, M. Gordon, G. Hanson, G. Karapostoli, O.R. Long, N. Manganelli, M. Olmedo Negrete, W. Si, S. Wimpenny, Y. Zhang

University of California, San Diego, La Jolla, U.S.A.

J.G. Branson, P. Chang, S. Cittolin, S. Cooperstein, N. Deelen, D. Diaz, J. Duarte, R. Gerosa, L. Giannini, D. Gilbert, J. Guiang, R. Kansal, V. Krutelyov, R. Lee, J. Letts, M. Masciovecchio, S. May, M. Pieri, B.V. Sathia Narayanan, V. Sharma, M. Tadel, A. Vartak, F. Würthwein, Y. Xiang, A. Yagil

University of California, Santa Barbara — Department of Physics, Santa Barbara, U.S.A.

N. Amin, C. Campagnari, M. Citron, A. Dorsett, V. Dutta, J. Incandela, M. Kilpatrick, J. Kim, B. Marsh, H. Mei, M. Oshiro, M. Quinnan, J. Richman, U. Sarica, F. Setti, J. Sheplock, D. Stuart, S. Wang

California Institute of Technology, Pasadena, U.S.A.

A. Bornheim, O. Cerri, I. Dutta, J.M. Lawhorn, N. Lu, J. Mao, H.B. Newman, T.Q. Nguyen, M. Spiropulu, J.R. Vlimant, C. Wang, S. Xie, Z. Zhang, R.Y. Zhu

Carnegie Mellon University, Pittsburgh, U.S.A.

J. Alison, S. An, M.B. Andrews, P. Bryant, T. Ferguson, A. Harilal, C. Liu, T. Mudholkar, M. Paulini, A. Sanchez, W. Terrill

University of Colorado Boulder, Boulder, U.S.A.

J.P. Cumalat, W.T. Ford, A. Hassani, E. MacDonald, R. Patel, A. Perloff, C. Savard, K. Stenson, K.A. Ulmer, S.R. Wagner

Cornell University, Ithaca, U.S.A.

J. Alexander, S. Bright-thonney, Y. Cheng, D.J. Cranshaw, S. Hogan, J. Monroy, J.R. Patterson, D. Quach, J. Reichert, M. Reid, A. Ryd, W. Sun, J. Thom, P. Wittich, R. Zou

Fermi National Accelerator Laboratory, Batavia, U.S.A.

M. Albrow, M. Alyari, G. Apollinari, A. Apresyan, A. Apyan, S. Banerjee, L.A.T. Bauerdick, D. Berry, J. Berryhill, P.C. Bhat, K. Burkett, J.N. Butler, A. Canepa, G.B. Cerati, H.W.K. Cheung, F. Chlebana, M. Cremonesi, K.F. Di Petrillo, V.D. Elvira, Y. Feng, J. Freeman, Z. Gecse, L. Gray, D. Green, S. Grünendahl, O. Gutsche, R.M. Harris, R. Heller, T.C. Herwig, J. Hirschauer, B. Jayatilaka, S. Jindariani, M. Johnson, U. Joshi, T. Klijnsma, B. Klima, K.H.M. Kwok, S. Lammel, D. Lincoln, R. Lipton, T. Liu, C. Madrid, K. Maeshima, C. Mantilla, D. Mason, P. McBride, P. Merkel, S. Mrenna, S. Nahn, J. Ngadiuba, V. O'Dell, V. Papadimitriou, K. Pedro, C. Pena[57], O. Prokofyev, F. Ravera, A. Reinsvold Hall, L. Ristori, B. Schneider, E. Sexton-Kennedy, N. Smith, A. Soha, W.J. Spalding, L. Spiegel, S. Stoynev, J. Strait, L. Taylor, S. Tkaczyk, N.V. Tran, L. Uplegger, E.W. Vaandering, H.A. Weber

JHEP11(2021)057

University of Florida, Gainesville, U.S.A.

D. Acosta, P. Avery, D. Bourilkov, L. Cadamuro, V. Cherepanov, F. Errico, R.D. Field, D. Guerrero, B.M. Joshi, M. Kim, E. Koenig, J. Konigsberg, A. Korytov, K.H. Lo, K. Matchev, N. Menendez, G. Mitselmakher, A. Muthirakalayil Madhu, N. Rawal, D. Rosenzweig, S. Rosenzweig, K. Shi, J. Sturdy, J. Wang, E. Yigitbasi, X. Zuo

Florida State University, Tallahassee, U.S.A.

T. Adams, A. Askew, R. Habibullah, V. Hagopian, K.F. Johnson, R. Khurana, T. Kolberg, G. Martinez, H. Prosper, C. Schiber, O. Viazlo, R. Yohay, J. Zhang

Florida Institute of Technology, Melbourne, U.S.A.

M.M. Baarmand, S. Butalla, T. Elkafrawy[90], M. Hohlmann, R. Kumar Verma, D. Noonan, M. Rahmani, F. Yumiceva

University of Illinois at Chicago (UIC), Chicago, U.S.A.

M.R. Adams, H. Becerril Gonzalez, R. Cavanaugh, X. Chen, S. Dittmer, O. Evdokimov, C.E. Gerber, D.A. Hangal, D.J. Hofman, A.H. Merrit, C. Mills, G. Oh, T. Roy, S. Rudrabhatla, M.B. Tonjes, N. Varelas, J. Viinikainen, X. Wang, Z. Wu, Z. Ye

The University of Iowa, Iowa City, U.S.A.

M. Alhusseini, K. Dilsiz[91], R.P. Gandrajula, O.K. Köseyan, J.-P. Merlo, A. Mestvirishvili[92], J. Nachtman, H. Ogul[93], Y. Onel, A. Penzo, C. Snyder, E. Tiras[94]

Johns Hopkins University, Baltimore, U.S.A.

O. Amram, B. Blumenfeld, L. Corcodilos, J. Davis, M. Eminizer, A.V. Gritsan, S. Kyriacou, P. Maksimovic, J. Roskes, M. Swartz, T.Á. Vámi

The University of Kansas, Lawrence, U.S.A.

A. Abreu, J. Anguiano, C. Baldenegro Barrera, P. Baringer, A. Bean, A. Bylinkin, Z. Flowers, T. Isidori, S. Khalil, J. King, G. Krintiras, A. Kropivnitskaya, M. Lazarovits, C. Lindsey, J. Marquez, N. Minafra, M. Murray, M. Nickel, C. Rogan, C. Royon, R. Salvatico, S. Sanders, E. Schmitz, C. Smith, J.D. Tapia Takaki, Q. Wang, Z. Warner, J. Williams, G. Wilson

Kansas State University, Manhattan, U.S.A.

S. Duric, A. Ivanov, K. Kaadze, D. Kim, Y. Maravin, T. Mitchell, A. Modak, K. Nam

Lawrence Livermore National Laboratory, Livermore, U.S.A.

F. Rebassoo, D. Wright

University of Maryland, College Park, U.S.A.

E. Adams, A. Baden, O. Baron, A. Belloni, S.C. Eno, N.J. Hadley, S. Jabeen, R.G. Kellogg, T. Koeth, A.C. Mignerey, S. Nabili, C. Palmer, M. Seidel, A. Skuja, L. Wang, K. Wong

Massachusetts Institute of Technology, Cambridge, U.S.A.

D. Abercrombie, G. Andreassi, R. Bi, S. Brandt, W. Busza, I.A. Cali, Y. Chen, M. D'Alfonso, J. Eysermans, C. Freer, G. Gomez Ceballos, M. Goncharov, P. Harris, M. Hu, M. Klute, D. Kovalskyi, J. Krupa, Y.-J. Lee, B. Maier, C. Mironov, C. Paus, D. Rankin, C. Roland, G. Roland, Z. Shi, G.S.F. Stephans, J. Wang, Z. Wang, B. Wyslouch

JHEP11(2021)057

University of Minnesota, Minneapolis, U.S.A.

R.M. Chatterjee, A. Evans, P. Hansen, J. Hiltbrand, Sh. Jain, M. Krohn, Y. Kubota, J. Mans, M. Revering, R. Rusack, R. Saradhy, N. Schroeder, N. Strobbe, M.A. Wadud

University of Nebraska-Lincoln, Lincoln, U.S.A.

K. Bloom, M. Bryson, S. Chauhan, D.R. Claes, C. Fangmeier, L. Finco, F. Golf, C. Joo, I. Kravchenko, M. Musich, I. Reed, J.E. Siado, G.R. Snow[†], W. Tabb, F. Yan

State University of New York at Buffalo, Buffalo, U.S.A.

G. Agarwal, H. Bandyopadhyay, L. Hay, I. Iashvili, A. Kharchilava, C. McLean, D. Nguyen, J. Pekkanen, S. Rappoccio, A. Williams

Northeastern University, Boston, U.S.A.

G. Alverson, E. Barberis, Y. Haddad, A. Hortiangtham, J. Li, G. Madigan, B. Marzocchi, D.M. Morse, V. Nguyen, T. Orimoto, A. Parker, L. Skinnari, A. Tishelman-Charny, T. Wamorkar, B. Wang, A. Wisecarver, D. Wood

Northwestern University, Evanston, U.S.A.

S. Bhattacharya, J. Bueghly, Z. Chen, A. Gilbert, T. Gunter, K.A. Hahn, Y. Liu, N. Odell, M.H. Schmitt, M. Velasco

University of Notre Dame, Notre Dame, U.S.A.

R. Band, R. Bucci, A. Das, N. Dev, R. Goldouzian, M. Hildreth, K. Hurtado Anampa, C. Jessop, K. Lannon, J. Lawrence, N. Loukas, D. Lutton, N. Marinelli, I. Mcalister, T. McCauley, C. Mcgrady, F. Meng, K. Mohrman, Y. Musienko[49], R. Ruchti, P. Siddireddy, A. Townsend, M. Wayne, A. Wightman, M. Wolf, M. Zarucki, L. Zygala

The Ohio State University, Columbus, U.S.A.

B. Bylsma, B. Cardwell, L.S. Durkin, B. Francis, C. Hill, M. Nunez Ornelas, K. Wei, B.L. Winer, B.R. Yates

Princeton University, Princeton, U.S.A.

F.M. Addesa, B. Bonham, P. Das, G. Dezoort, P. Elmer, A. Frankenthal, B. Greenberg, N. Haubrich, S. Higginbotham, A. Kalogeropoulos, G. Kopp, S. Kwan, D. Lange, M.T. Lucchini, D. Marlow, K. Mei, I. Ojalvo, J. Olsen, D. Stickland, C. Tully

University of Puerto Rico, Mayaguez, U.S.A.

S. Malik, S. Norberg

Purdue University, West Lafayette, U.S.A.

A.S. Bakshi, V.E. Barnes, R. Chawla, S. Das, L. Gutay, M. Jones, A.W. Jung, S. Karmarkar, M. Liu, G. Negro, N. Neumeister, G. Paspalaki, C.C. Peng, S. Piperov, A. Purohit, J.F. Schulte, M. Stojanovic[16], J. Thieman, F. Wang, R. Xiao, W. Xie

Purdue University Northwest, Hammond, U.S.A.

J. Dolen, N. Parashar

JHEP11(2021)057

Rice University, Houston, U.S.A.

A. Baty, M. Decaro, S. Dildick, K.M. Ecklund, S. Freed, P. Gardner, F.J.M. Geurts, A. Kumar, W. Li, B.P. Padley, R. Redjimi, W. Shi, A.G. Stahl Leiton, S. Yang, L. Zhang, Y. Zhang

University of Rochester, Rochester, U.S.A.

A. Bodek, P. de Barbaro, R. Demina, J.L. Dulemba, C. Fallon, T. Ferbel, M. Galanti, A. Garcia-Bellido, O. Hindrichs, A. Khukhunaishvili, E. Ranken, R. Taus

Rutgers, The State University of New Jersey, Piscataway, U.S.A.

B. Chiarito, J.P. Chou, A. Gandrakota, Y. Gershtein, E. Halkiadakis, A. Hart, M. Heindl, O. Karacheban[23], I. Laflotte, A. Lath, R. Montalvo, K. Nash, M. Osherson, S. Salur, S. Schnetzer, S. Somalwar, R. Stone, S.A. Thayil, S. Thomas, H. Wang

University of Tennessee, Knoxville, U.S.A.

H. Acharya, A.G. Delannoy, S. Fiorendi, S. Spanier

Texas A&M University, College Station, U.S.A.

O. Bouhali[95], M. Dalchenko, A. Delgado, R. Eusebi, J. Gilmore, T. Huang, T. Kamon[96], H. Kim, S. Luo, S. Malhotra, R. Mueller, D. Overton, D. Rathjens, A. Safonov

Texas Tech University, Lubbock, U.S.A.

N. Akchurin, J. Damgov, V. Hegde, S. Kunori, K. Lamichhane, S.W. Lee, T. Mengke, S. Muthumuni, T. Peltola, I. Volobouev, Z. Wang, A. Whitbeck

Vanderbilt University, Nashville, U.S.A.

E. Appelt, S. Greene, A. Gurrola, W. Johns, A. Melo, H. Ni, K. Padeken, F. Romeo, P. Sheldon, S. Tuo, J. Velkovska

University of Virginia, Charlottesville, U.S.A.

M.W. Arenton, B. Cox, G. Cummings, J. Hakala, R. Hirosky, M. Joyce, A. Ledovskoy, A. Li, C. Neu, B. Tannenwald, S. White, E. Wolfe

Wayne State University, Detroit, U.S.A.

N. Poudyal

University of Wisconsin — Madison, Madison, WI, U.S.A.

K. Black, T. Bose, J. Buchanan, C. Caillol, S. Dasu, I. De Bruyn, P. Everaerts, F. Fienga, C. Galloni, H. He, M. Herndon, A. Hervé, U. Hussain, A. Lanaro, A. Loeliger, R. Loveless, J. Madhusudanan Sreekala, A. Mallampalli, A. Mohammadi, D. Pinna, A. Savin, V. Shang, V. Sharma, W.H. Smith, D. Teague, S. Trembath-Reichert, W. Vetens

†: Deceased

1: Also at TU Wien, Wien, Austria

2: Also at Institute of Basic and Applied Sciences, Faculty of Engineering, Arab Academy for Science, Technology and Maritime Transport, Alexandria, Egypt, Alexandria, Egypt

3: Also at Université Libre de Bruxelles, Bruxelles, Belgium

4: Also at Universidade Estadual de Campinas, Campinas, Brazil

JHEP11(2021)057

5: Also at Federal University of Rio Grande do Sul, Porto Alegre, Brazil
6: Also at University of Chinese Academy of Sciences, Beijing, China
7: Also at Department of Physics, Tsinghua University, Beijing, China, Beijing, China
8: Also at UFMS, Nova Andradina, Brazil
9: Also at Nanjing Normal University Department of Physics, Nanjing, China
10: Now at The University of Iowa, Iowa City, U.S.A.
11: Also at Institute for Theoretical and Experimental Physics named by A.I. Alikhanov of NRC 'Kurchatov Institute', Moscow, Russia
12: Also at Joint Institute for Nuclear Research, Dubna, Russia
13: Also at Cairo University, Cairo, Egypt
14: Also at Helwan University, Cairo, Egypt
15: Now at Zewail City of Science and Technology, Zewail, Egypt
16: Also at Purdue University, West Lafayette, U.S.A.
17: Also at Université de Haute Alsace, Mulhouse, France
18: Also at Erzincan Binali Yildirim University, Erzincan, Turkey
19: Also at CERN, European Organization for Nuclear Research, Geneva, Switzerland
20: Also at RWTH Aachen University, III. Physikalisches Institut A, Aachen, Germany
21: Also at University of Hamburg, Hamburg, Germany
22: Also at Department of Physics, Isfahan University of Technology, Isfahan, Iran, Isfahan, Iran
23: Also at Brandenburg University of Technology, Cottbus, Germany
24: Also at Skobeltsyn Institute of Nuclear Physics, Lomonosov Moscow State University, Moscow, Russia
25: Also at Physics Department, Faculty of Science, Assiut University, Assiut, Egypt
26: Also at Karoly Robert Campus, MATE Institute of Technology, Gyongyos, Hungary
27: Also at Institute of Physics, University of Debrecen, Debrecen, Hungary, Debrecen, Hungary
28: Also at Institute of Nuclear Research ATOMKI, Debrecen, Hungary
29: Also at MTA-ELTE Lendület CMS Particle and Nuclear Physics Group, Eötvös Loránd University, Budapest, Hungary, Budapest, Hungary
30: Also at Wigner Research Centre for Physics, Budapest, Hungary
31: Also at IIT Bhubaneswar, Bhubaneswar, India, Bhubaneswar, India
32: Also at Institute of Physics, Bhubaneswar, India
33: Also at G.H.G. Khalsa College, Punjab, India
34: Also at Shoolini University, Solan, India
35: Also at University of Hyderabad, Hyderabad, India
36: Also at University of Visva-Bharati, Santiniketan, India
37: Also at Indian Institute of Technology (IIT), Mumbai, India
38: Also at Deutsches Elektronen-Synchrotron, Hamburg, Germany
39: Also at Sharif University of Technology, Tehran, Iran
40: Also at Department of Physics, University of Science and Technology of Mazandaran, Behshahr, Iran
41: Now at INFN Sezione di Bari [a], Università di Bari [b], Politecnico di Bari [c], Bari, Italy
42: Also at Italian National Agency for New Technologies, Energy and Sustainable Economic Development, Bologna, Italy
43: Also at Centro Siciliano di Fisica Nucleare e di Struttura Della Materia, Catania, Italy
44: Also at Università di Napoli 'Federico II', Napoli, Italy
45: Also at Consiglio Nazionale delle Ricerche — Istituto Officina dei Materiali, Perugia, Italy
46: Also at Riga Technical University, Riga, Latvia, Riga, Latvia
47: Also at Consejo Nacional de Ciencia y Tecnología, Mexico City, Mexico

JHEP11(2021)057

48: Also at IRFU, CEA, Université Paris-Saclay, Gif-sur-Yvette, France
49: Also at Institute for Nuclear Research, Moscow, Russia
50: Now at National Research Nuclear University 'Moscow Engineering Physics Institute' (MEPhI), Moscow, Russia
51: Also at Institute of Nuclear Physics of the Uzbekistan Academy of Sciences, Tashkent, Uzbekistan
52: Also at St. Petersburg State Polytechnical University, St. Petersburg, Russia
53: Also at University of Florida, Gainesville, U.S.A.
54: Also at Imperial College, London, United Kingdom
55: Also at Moscow Institute of Physics and Technology, Moscow, Russia, Moscow, Russia
56: Also at P.N. Lebedev Physical Institute, Moscow, Russia
57: Also at California Institute of Technology, Pasadena, U.S.A.
58: Also at Budker Institute of Nuclear Physics, Novosibirsk, Russia
59: Also at Faculty of Physics, University of Belgrade, Belgrade, Serbia
60: Also at Trincomalee Campus, Eastern University, Sri Lanka, Nilaveli, Sri Lanka
61: Also at INFN Sezione di Pavia [a], Università di Pavia [b], Pavia, Italy, Pavia, Italy
62: Also at National and Kapodistrian University of Athens, Athens, Greece
63: Also at Ecole Polytechnique Fédérale Lausanne, Lausanne, Switzerland
64: Also at Universität Zürich, Zurich, Switzerland
65: Also at Stefan Meyer Institute for Subatomic Physics, Vienna, Austria, Vienna, Austria
66: Also at Laboratoire d'Annecy-le-Vieux de Physique des Particules, IN2P3-CNRS, Annecy-le-Vieux, France
67: Also at Şırnak University, Sirnak, Turkey
68: Also at Near East University, Research Center of Experimental Health Science, Nicosia, Turkey
69: Also at Konya Technical University, Konya, Turkey
70: Also at Istanbul University — Cerrahpasa, Faculty of Engineering, Istanbul, Turkey
71: Also at Piri Reis University, Istanbul, Turkey
72: Also at Adiyaman University, Adiyaman, Turkey
73: Also at Ozyegin University, Istanbul, Turkey
74: Also at Izmir Institute of Technology, Izmir, Turkey
75: Also at Necmettin Erbakan University, Konya, Turkey
76: Also at Bozok Universitetesi Rektörlügü, Yozgat, Turkey, Yozgat, Turkey
77: Also at Marmara University, Istanbul, Turkey
78: Also at Milli Savunma University, Istanbul, Turkey
79: Also at Kafkas University, Kars, Turkey
80: Also at Istanbul Bilgi University, Istanbul, Turkey
81: Also at Hacettepe University, Ankara, Turkey
82: Also at Rutherford Appleton Laboratory, Didcot, United Kingdom
83: Also at Vrije Universiteit Brussel, Brussel, Belgium
84: Also at School of Physics and Astronomy, University of Southampton, Southampton, United Kingdom
85: Also at IPPP Durham University, Durham, United Kingdom
86: Also at Monash University, Faculty of Science, Clayton, Australia
87: Also at Università di Torino, Torino, Italy
88: Also at Bethel University, St. Paul, Minneapolis, U.S.A., St. Paul, U.S.A.
89: Also at Karamanoğlu Mehmetbey University, Karaman, Turkey
90: Also at Ain Shams University, Cairo, Egypt

JHEP11(2021)057

91: Also at Bingol University, Bingol, Turkey
92: Also at Georgian Technical University, Tbilisi, Georgia
93: Also at Sinop University, Sinop, Turkey
94: Also at Erciyes University, Kayseri, Turkey
95: Also at Texas A&M University at Qatar, Doha, Qatar
96: Also at Kyungpook National University, Daegu, Korea, Daegu, Korea

JHEP11(2021)057